University of Stavanger

Faculty of Science and Technology

MASTER'S THESIS

Study program/Specialization: Petroleum Engineering	Spring semester, 2016 Open
Writer: Kristian Stangeland	...Kristian Stangeland..... (Writer's signature)
Faculty supervisor: Prof. Zhixin Yu	
Tittel på masteroppgaven: Tørr reforming av metan over nikkel baserte katalysatorer modifisert med edle metaller Thesis title: Dry reforming of methane over nickel based catalysts modified with noble metals	
Credits (ECTS): 60	
Key words: Dry reforming of Methane Supported Metal Catalyst Nickel based catalyst Noble Metal Modified Ni Catalysts Catalyst Activation Catalyst characterization	Pages: 73 Stavanger, 01/07/2016

Acknowledgment

First and foremost, I would like to thank my supervisor Professor Zhixin Yu and Dori Kalai for their support and dedication in leading me throughout this work.

The Petroleum Technology bachelor program and the Natural Gas and Production master program consists to a limited degree of chemical related subjects. I was thus first directly introduced to chemical engineering through Pr. Yu's course Natural Gas Conversion during the autumn semester of 2015. The course presented a fascinating field of chemical engineering which spiked an interest and convinced me to pursue writing a master thesis within the field.

There has been a lot of challenges along the way regarding the experimental setup. The setup was still in development and it has been interesting to have taken a small part of its development. The late date of completion for the setup and delivery of experimental equipment led to experiments being conducted even within the final days prior to the due date of the thesis. Overall the journey has been exciting and the challenges related to the experiments have been interesting.

Many thanks also for the generous help from employees at the Department of Petroleum Engineering in supplying expertise and help to solve problems that arose as fast as possible.

Finally, many thanks to my family who has support and helped me throughout my studies.

Abstract

Recently there has been renewed attention in dry reforming of methane (DRM) due to potential environmental benefits of utilizing CO_2 and an increase in demand for synthesis gas. DRM refers to the chemical reaction of methane and carbon dioxide to form hydrogen and carbon monoxide which are designated as synthetic gas (syngas). Syngas is primarily produced from a catalytic steam reforming process where the resulting H_2/CO product ratio is higher than the ratio required for many down-stream processes. DRM produce a syngas with a H2/CO ratio close to unity, making it an ideal feed for the Fischer-Tropsch process and highly selective syntheses of a wide range of chemicals.

The DRM utilizes CO2 as an oxidant to react methane over a heterogeneous catalyst. Group VIII metal catalysts have been extensively studied for DRM. Both noble metals (e.g. Ru, Rh, Pt, Pd) and non-noble metals (e.g. Ni, Fe, Co) have been found to be catalytically active towards this reaction. The main problem in DRM is related to catalyst deactivation due to sintering and carbon deposition. Although noble metal based catalysts are usually highly active, stable at high temperatures and experience low carbon formation, they have the drawbacks of high cost and limited availability. Hence, a more promising alternative is to incorporate small amounts of noble metals into non-noble metal catalysts.

Here, we report DRM over nickel alumina catalysts prepared by incipient wetness. The effect of modifying the catalyst with small amounts of Rh, Ru, Pt and Pd were studied. Two nickel catalysts on different alumina supports have also been investigated for comparison. The nickel loading was kept constant at 12 wt% for all the catalysts and the modified catalysts had a loading of 12 wt% Ni and 0.5 wt% noble metal. The characteristics of the catalysts were investigated by X-Ray diffraction (XRD), textural measurements, active metal dispersion and temperature-programmed reduction. Results from the XRD showed that the particle size was affected by the support and reduced by the noble metals. The textural measurement indicated similar surface area, were a slight reduction was observed for the modified catalysts. Indications from the TPR analysis suggested that characteristics of the support has a high impact on the reducibility of Ni based catalysts.

The activity and stability was investigated in a fixed-bed stainless steel reactor. The catalysts were activated at 600 ^oC and the DRM reactions were carried out at 700 ^oC at equimolar reactant feed and a gas hour space velocity of 120,000 $Scm^3\,g^{-1}\,h^{-1}$. The stability of the catalyst was investigated for 15 hours. The activity of monometallic Ni catalyst was found to be dependent on the support and improvements were observed for the catalysts modified with Rh, Pt and Ru, while Pd showed reduced activity. In addition, the Rh modified catalyst was investigated at 650 and 600 ^oC to determine the effect of temperature. The deactivation rate and H_2/CO ratio was found to decrease with temperature, which contradicts thermodynamic equilibrium calculations. Further research to optimize the noble metal catalyst is suggested through a higher extent of bimetallic particle control.

Table of Contents

List of Figures

List of Tables

1 Introduction

1.1 Background

Natural gas reserves are abundant, and todays discovered reserves equals about 200 years of supply at current demand. Natural gas is presently one of the cheapest sources of energy available [1]. A vast amount of additional natural gas has been discovered through unconventional gas (e.g. unconventional shale gas from North America) and is starting to be produced. The increase in production is expected to help maintain a low gas price in the future, which is beneficial in regards to utilizing natural gas as a feedstock for the petrochemical industry. Concerns related to the impact that CO2 might have on the climate could further facilitate the use of natural gas. Increasing concentration of Greenhouse gases (GHGs) in the atmosphere is proposed to have a negative effect on the climate, causing the global surface temperature to increase. Natural gas is the cleanest fossil fuel available and could be used to reduce CO_2 emissions in sectors where oil and coal is used as the primary source of energy.

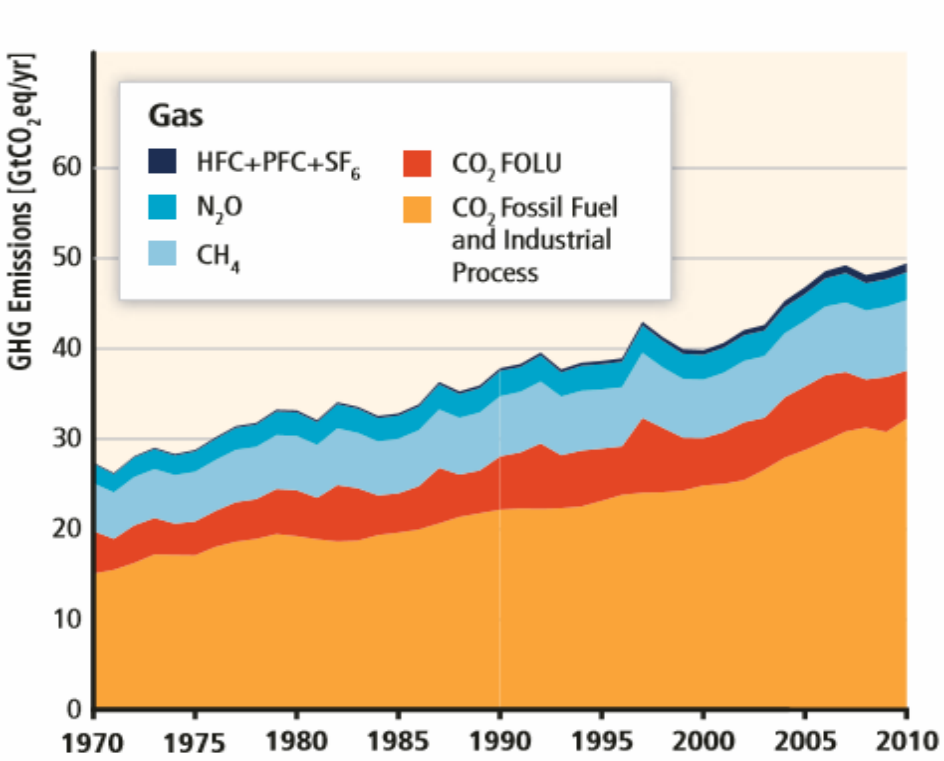

Figure 1.1: Total gas emissions based on CO_2 equivalent *[2]*

GHG emissions are strongly related to world population growth and consequently the growing energy demand. The European commission has committed to reduce GHG emissions, where the latest agreement has been a minimum of 40% cuts in GHG emissions from 1990 levels by 2030 [3]. Natural gas has the potential to reduce GHG emissions and at the same time meet the growing energy demand. Furthermore, natural gas can be used to produce synthetic fuels and chemicals, increasing its potential for utilization.

One strategy to reduce emissions of CO_2 is carbon capture and storage (CCS). CCS involves capturing CO_2 from natural gas fields or large industrial pants, compressing it for transportation and then injecting it into a safe location for storage. Possible CO_2 storage sites are producing oil fields, depleted oil and gas fields and saline aquifers. In Norway a detailed analysis of the storage capacity has been conducted [4].

Although CCS provides a relatively effective option for CO_2 emission reduction, it has certain limitations [5]. It requires a high geological storage capacity and a method of transporting the CO_2 from the source to the storage location, as well a high capture cost, which could require a high capital investment cost. There is also public resistance to CCS, which could preclude certain storage locations (e.g. storage under land). To overcome these concerns and potentially add value to the carbon value chain, parts of the CO_2 could be utilized, for example by application in enhanced oil recovery or by converting them to fuels and chemicals.

Reforming of natural gas produces a syngas consisting of H_2 and CO, which is already being used to produce a range of different products (Fig. 1.2). Different reforming technologies results in different H_2/CO ratios. CO_2 reforming of methane has a theoretical H_2/CO ratio of one, which is lower than the typical H_2/CO ratio for steam methane reforming (SRM), autothermal reforming (ATR) and partial oxidation of methane (POM).

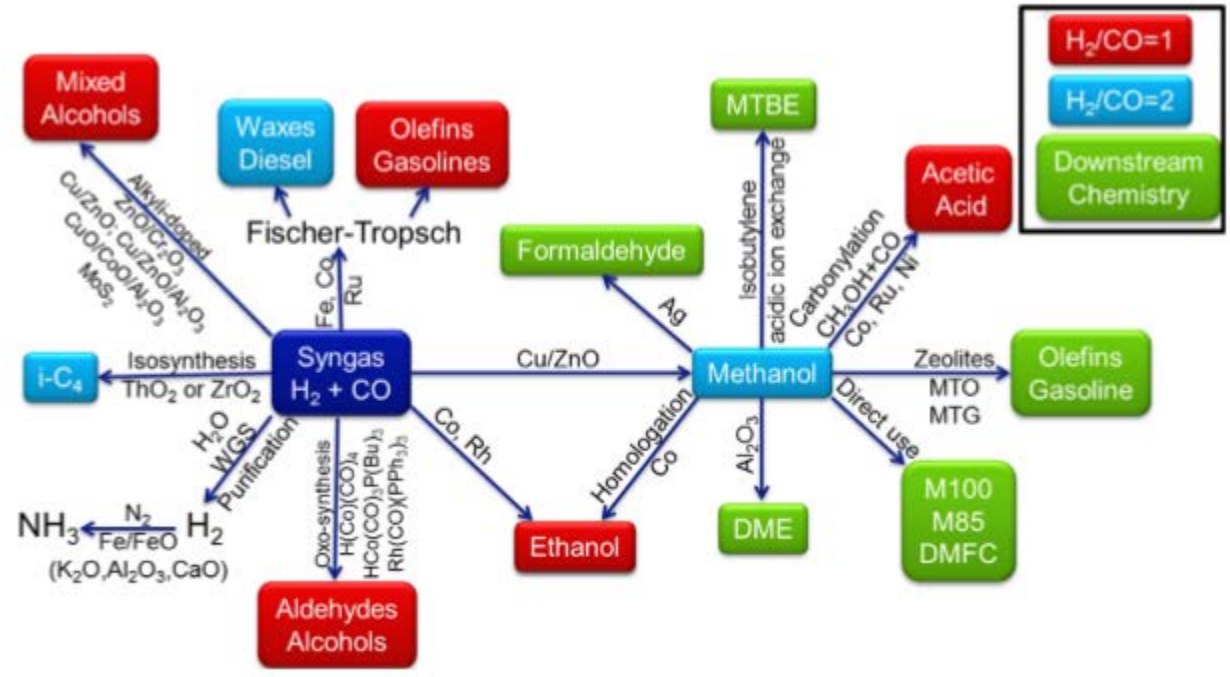

Figure 1.2: Use of syngas in the chemical industry *[6]*

1.2 Overview of Reforming Technologies

Reforming of methane is done by oxidation, which results in a synthesis gas consisting of mainly CO and H_2. In most reforming processes, a heterogeneous catalyst is used to enhance the process. The three oxidizing agents used in reforming are H_2O in steam methane reforming (SMR), O_2 in partial oxidation of methane (POX) and CO_2 in dry reforming of methane (DRM).

Autothermal reforming (ATR) can be considered to be a combination of of a partial oxydation and steam reforming.

1.2.1 Steam Methane Reforming

SMR is an endothermic process, which is widely used in the industry. It produces syngas by reacting high temperature steam with natural gas over a catalyst (Eq. 1.1). Further H_2 is produced through shift reactions following the main reactor, normally one high temperature shift reaction and one low temperature shift reaction, where the water gas shift reaction (Eq. 1.2) takes place to increase the yield of H_2.

$$\mathrm{CH_4 + H_2O \leftrightarrow CO + 3H_2} \qquad \Delta H^0_{298K} = 206\ \mathrm{kJ \cdot mol^{-1}} \qquad (1.1)$$

$$\mathrm{CO + H_2O \leftrightarrow CO_2 + H_2} \qquad \Delta H^0_{298K} = 163\ \mathrm{kJ \cdot mol^{-1}} \qquad (1.2)$$

The syngas produced has a H_2/CO ratio of about 3, which is higher than needed for Fischer-Tropsch (FT) synthesis of high value products. However, the high H_2 content of the syngas also makes it a viable H_2 source that could be used for e.g. the ammonia process or hydrogenation in refineries. A high amount of heat is required to drive the endothermic reaction, leading to high process costs. Operational costs and energy consumption are also increased when excess steam is used to inhibit catalyst deactivation due to carbon deposition [7].

1.2.2 Partial Oxidation of Methane

POX is an exothermic process where natural gas is partially combusted with oxygen (Eq. 1.3 and 1.4). Typical operating temperature for POX is 1200 – 1500 ˚C and 25-80 bar. Catalytic partial oxidation (CPOX) of methane mixes methane and oxygen before it is led to a catalyst bed. The use of a catalyst lowers the required reaction temperature to around 800 – 900˚C. POX and CPOX yields a H_2/CO ratio of about 2 [8].

$$\mathrm{CH_4 + \frac{1}{2}O_2 \leftrightarrow CO + 2H_2} \qquad \Delta H^0_{298K} = -32\ \mathrm{kJ \cdot mol^{-1}} \qquad (1.3)$$

$$\mathrm{CH_4 + O_2 \leftrightarrow CO_2 + 2H_2O} \qquad \Delta H^0_{298K} = -802\ \mathrm{kJ \cdot mol^{-1}} \qquad (1.4)$$

Due to being an exothermic reaction, POX has an economical advantage compared to SMR and DRM from one perspective. In most cases a pure source of O_2 is needed, which could lead to higher costs in the form of the O_2 source and necessary precautionary measures related to the risk of explosion [9].

1.2.3 Autothermal Reforming

An ATR contains a combustion zone at the top and a catalyst bed at the bottom of the reactor. The natural gas is premixed with a sub-stoichiometric amount of oxygen and steam before being

ignited in the combustion zone (Eq 1.3 and 1.4). The hot gasses continue to react through the reactor, but are far from equilibrium as they approach the catalyst bed. Reaction 1.1 and 1.5 occurs as the gasses pass through the catalyst and exit close to equilibrium. The temperature in the combustion zone is approximately 2000 ^{o}C and in the reforming zone 900 - 1100 ^{o}C [8]. Figure 1.3 shows a schematic of a typical ATR reactor.

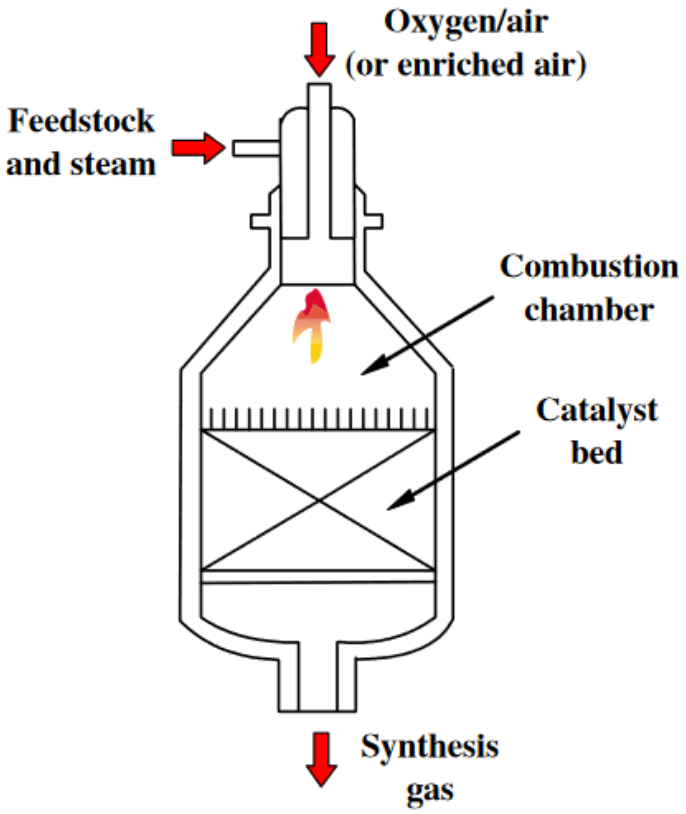

Figure 1.3: Diagram of an ATR [9]

ATR can produce a H_2/CO ratio of 1 to 2 and is therefore a more flexible option compared to other reforming technologies [10]. The compact reactor offers moderate cost, size and weight requirements. Steam must be added to avoid the formation of soot during combustion, and it contributes to higher costs. An extensive control system for mixing the gases is also required to control the reaction. In addition, the high temperature of the gas mixture entering the catalyst bed requires a catalyst and carrier system with high thermal stability [11].

1.2.4 Dry Reforming of Methane

In DRM methane reacts with CO2 to produce syngas over a heterogeneous catalyst. DMR is slightly more endothermic than SMR and is favored by low pressure and high temperature [12]. Simplistically, DRM consists of a main reaction (Eq. 1.5) and three side reactions (table 1): Methane decomposition (Eq. 1.6), Boudouard reaction (Eq. 1.7) and Revers Water Gas shift (RWGS) reaction (Eq. 1.8). Methane Decomposition and Boudouard reaction are proposed to be

the main reactions leading to carbon deposition depending on pressure, temperature and feed gas ratio.

Table 1.1: The DRM reactions

Reaction Designation	Reaction	ΔH^0_{298K} $kJ \cdot mol^{-1}$	ΔG^0	Reaction priority	Eq.
DRM	$CH_4 + CO_2 \leftrightarrow 2CO + 2H_2$	247	61770-67.32T	Main Reaction	(1.5)
Methane Decomposition (Methane Cracking)	$CH_4 \leftrightarrow C + 2H_2$	75	29960-26.45T	Side Reaction	(1.6)
Boudouard (CO Disproportionation)	$2CO \leftrightarrow CO_2 + C$	-171	-39810+40.87T	Side reaction	(1.7)
Revers Water Gas Shift (RWGS)	$CO_2 + H_2 \leftrightarrow CO + H_2O$	41	-8545+7.84T	Side Reaction	(1.8)

Based on the Gibbs free energy from equation (1.5) to (1.8) [13], the thermodynamics of the reactions involved in DRM are shown in Figure 1.4.

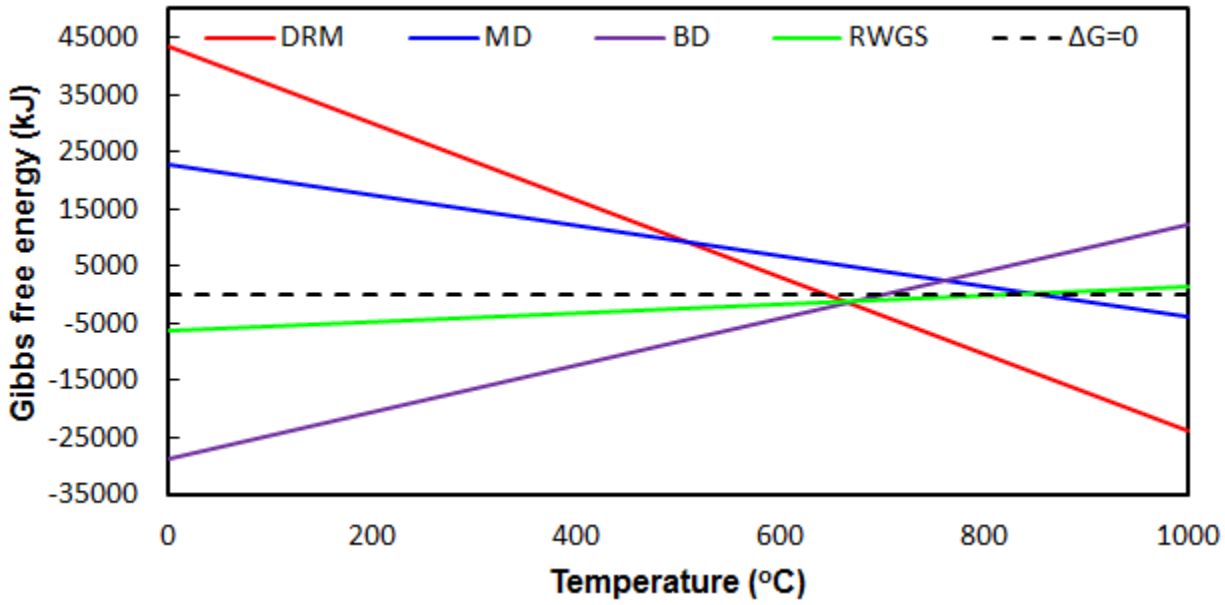

Figure 1.4: Plot depicting the variation of Gibbs free energy (KJ) with temperature (˚C) based on values in Table 1.1 for dry reforming of methane (DRM), Methane decomposition (MD), Boudouard reaction (BR) and reverse water gas shift (RWGS). Red line indicates ΔG=0.

It can be seen that the DRM and methane decomposition (MD) reactions become thermodynamically more favored as the temperature increases. The DRM reaction is favored by low pressure based on the stoichiometry of the reaction and Le Chatelier's principle. On the other hand, the Boudouard reaction (BR) and the RWGS are favored with decreasing temperature. It is

worth mentioning that operating at low pressure is not favored in industrial applications, where it would require a large reactor and recompression for downstream processes. However, increasing the pressure leads to an increase in carbon deposition [14].

One of the advantages of DRM is a lower H_2/CO ratio (about 1) that for instance could be advantageous in FT synthesis. Excess H_2 suppress chain growth and decrease the selectivity of higher hydrocarbons in the FT process [15]. DRM also consumes both CO_2 and CH_4 which are two abundantly available greenhouse gases. As DRM is highly endothermic, the source of energy used to supply heat is of importance when considering CO_2 emissions. It could therefore be useful in energy transmission systems to store excess energy from renewable sources (e.g. solar [16]). Natural gas reserves and biogas with a high CO_2 content could potentially be used directly for DRM and potentially add value to the project. The main challenge in DRM is related to catalyst deactivation, mainly due to significant carbon deposition on the surface of the catalyst.

1.3 Scope of the present work

The objective of this work was to: a) compare alumina supported nickel based catalysts with modified catalysts with small amounts of noble metals, b) Conclude and suggest further focus in catalyst development.

The following steps were taken to attain this objective:

1) Synthesize through incipient wetness method monometallic nickel based catalysts over two different supports and also bimetallic nickel based catalysts with low amounts of noble metal.

2) Characterize the catalysts: a) physically for crystallinity using X-ray diffraction (XRD), surface area through Brunauer Emmett Teller (BET) method, b) chemically for bulk metallic reduction using Temperature Programmed Reduction (TPR) and metallic dispersion and active species particle size using chemisorption.

3) Test the catalyst in a laboratory scaled fixed-bed stainless steel reactor at temperature of 600, 650 and 700 ^{o}C, at atmospheric pressure and GHSV of 120,000 $Scm^3\ g^{-1}\ h^{-1}$.

4) Analyze the converted gases by TCD gas chromatography.

2 Literature Review: DRM Catalysts

2.1 Nickel Based Catalyst

The active metals used in DRM belong to Group VIII and are divided into earth-abundant transition metals and noble metals. Ni has shown the highest activity of the non-noble metals, and is the most widely studied active metal for DRM. However, it suffers from rapid deactivation due to carbon deposits [17, 18]. The carbon deposits are proposed originate from methane cracking (Eq. 1.6) and/or CO disproportionation (Eq. 1.7) and depends on the thermodynamic variables and active metal species [19].

The deposited carbon can have different structural order, morphology, and reactivity, depending on the specific reaction conditions and structure of the catalyst [20]. The main types of carbon formed in DRM on supported metal catalysts are; polymeric, filamentous (e.g. whisker carbon), graphitic and bulk carbon [21, 22]. Polymeric coke is proposed to derive from thermal decomposition of hydrocarbons, whereas the filamentous and graphitic forms of coke are formed on the catalyst. Studies have revealed that the nickel crystallite size have significant effects on the degree of carbon formation on the catalyst, where smaller particles are more resistant to carbon formation [23, 24, 25]. In literature, both 10 nm and 7 nm have been suggested as the critical size for metallic nickel particles to inhibit carbon formation [26]. Amorphous carbon has been reported the most active and can rapidly be consumed by the Boudouard reaction (Eq. 1.7). Whereas the filamentous and graphitic types of carbon are proposed to not block active sites, but are consumed at a lesser rate than amorphous carbon. It has been suggested that bulk carbon causes a rapid loss of activity through physical coverage of the active sites, and that it is not consumed in the Boudouard reaction [27].

The size of the nickel particles is also important for catalytic activity which is related to the available nickel surface area. Smaller particles will yield a higher surface area compared to larger particles when the same amount of Ni loading is considered. Metal sintering is a process which leads to particle growth and occurs at temperatures lower than the metals melting point. The Tammann temperature is the temperature at which the atoms or molecules of the solid metal phase acquire sufficient energy for bulk mobility and the Tammann temperature for Nickel is 591^{o}C [28]. Surface diffusion happens at even lower temperature than the Tammann temperature. DRM is normally operated at high temperatures (600-800^{o}C), and sintering is considered as one of the problems in DRM. The growth of the Ni particles reduceses the activity of the catalyst, directly by reducing the surface area and indirectly by increasing the carbon formation rate.

The durability of the catalyst is related to the stability of the nickel particles and the carbon formation rate. The relationship between nickel particle size and carbon formation rate was investigated by thermogravimetric analysis experiments (TGA) [25] where the two catalysts had different mean nickel particle size (1020 Å, 15 wt% Ni loading and 70 Å, 0.92 wt%), but similar Ni surface area, pore system and activity. They found that the onset temperature for carbon formation was approximately 100 K higher for the smaller 70 Å Ni particles and that the carbon formation rate was much smaller (Figure 2.1).

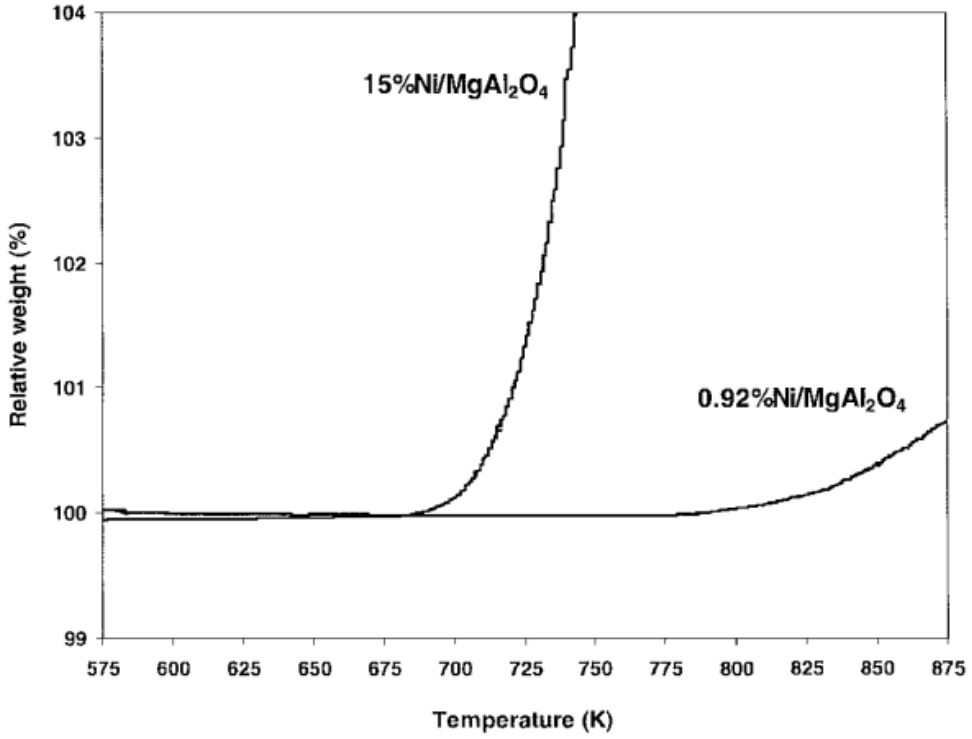

Figure 2.1: Relative weight increase as function of temperature for two Ni catalysts determined by TGA *[25]*

There are different carbon species that can be formed on the catalyst with different reactivity. Carbon growth will progressively encapsulate the Ni particles, hindering access to active sites and thereby reducing the activity [29]. Severe carbon deposition could lead to blockage of the pores, which in turn could hinder the flow through the catalyst and force the catalyst to be changed. In addition to the carbon formed on the catalyst, overheated gas film at the tube wall can act as a source of radicals and coal precursors, which in turn can lead to carbon formation along the tube wall of the reactor [28].

Although less attention is often given to the role of the support, it can have a significant effect on the overall catalytic behavior. A range of different supports has been tested for DRM. The supports role to disperse and stabilize the active metal is important to achieve a catalyst with high activity and long-term stability. Supports based on silicates and aluminates have been two of the most often investigated supports for DRM [30], but research is being done using different support to improve the catalyst. Under DRM conditions, migration of adsorbed species from the active metal to the support and vice versa can take place. It is evident that the support thereby can play a role in the DRM reactions [31]. One of the factors involved in the carbon deposition is the catalyst surface basicity [32]. Different supports have different acidic/basic properties. The basic sites of the support can improve the adsorption and dissociation of the acidic CO_2 [33]. One of its effects is an increase in available oxygen that can increase the regasification rate of deposited carbon and thereby enhance the durability. The basicity can also have an impact on the overall oxygen mobility, which is connected to the catalyst ability to transfer oxygen to the deposited carbon. The size of the Ni particles is suggested to be connected to the overall participation of the support through the metal-support interfacial zone [34], implying that small Ni particle size has a

synergetic effect with the support. It appears that detailed analysis of the supports contribution is often overlooked and problematic to determine. In any case the tuning of the interaction between the active metal and support appears to be challenging and of importance for optimal catalytic properties.

Further improvements can be done through catalyst promoters [35], which are substances that are added in small amounts to improve the catalytic performance. Different promoters have different effects and the added amount is often of importance. One example is potassium, and a study on potassium promoted Ni/MgO-ZrO_2 showed improved thermal stability and resistance to deactivation with increasing loading reaching an optimum at 0.5 wt.% [36]. The different promoters offer a diversity of effects, including enhanced metal dispersion over the support [37], blocking step sites on the nickel particles thereby disrupting coke formation, improving regasification rate of carbon, improving stability of the active metal and altering the type of formed coke (e.g. Ag [38]).

Research is also being conducted on the effects of the preparation method [38] and using advanced reactor configurations [39]. It is evident that there are several factors that affect the catalyst's performance in each step, from catalyst preparation to catalyst reactor setup. In the case of Ni based catalyst, the need for small Ni particles highly dispersed and stabilized on the support is evident, but remains a challenge.

2.2 Nobel Metals in DRM

Numerous studies have been done on monometallic noble metal catalysts. Noble metals exhibit higher resistance to coking, high activity for dry reforming and are highly stable at high temperature applications [40]. Metal sintering is related to the Tammann temperature (Table 2.1) and on this basis rhodium, ruthenium and iridium are superior to Ni in terms of particle stability against sintering.

Table 2.1: Tammann temperatures of common metals used in DRM

Metal	Tammann temperature	Metal	Tammann Temperature
Fe	630 °C	**Co**	610 °C
Ni	590 °C	**Pt**	750 °C
Pd	640 °C	**Rh**	845 °C
Ru	990 °C	**Ir**	1085 °C

To investigate sintering of platinum, a $PtAl_2O_3$ catalyst prepared by the sol-gel method was used [41]. The catalyst was heated in air at 700 °C. The results showed a rapid growth in particle size where the mean diameter increased from 50 to 300 Å after 8 hours. The catalyst stability is of importance and one would expect that the sintering observed in this case would lead to rapid deactivation, rendering the catalyst not suitable in DRM applications.

On the other hand, nanoparticles of Ru supported on y-AlO3 was subjected to heat treatment in hydrogen up to 700 °C [42]. It was found that the particles were stable up to 500 °C and minor

sintering of Ru occurred at 600-700 ºC. A general conclusion so far is that the Tamman Temperature gives a good indication of the metals stability. Although as previously mentioned for Ni, there are several other factors that must be considered that could affect the stability of the catalytic particles.

In literature, studies of noble metal catalyst have revealed inconsistencies in the results presented by different groups [43]. A comparison of noble metals (5 wt%) supported by Al_2O_3 was conducted by Hou et al. [44]. The catalysts showed high coking resistance and stability in the order of Rh>Ru>Ir>Pd>Pt and was in agreement with the findings of Matsui [45]. The relatively lower stability of Pt and Pd supported catalysts is attributed to sintering of the metal particles [46].

The support is known to affect the performance of the catalyst, and that different supports function differently with the active metals [46]. Moreover, it is evident that this is the case for noble metal catalysts, and the support contribution can be in the form of altering the reaction mechanism. Ferreira et al [43] investigated a Ru/γ-Al_2O_3 catalyst and found that CO_2 is more efficiently activated on the support through the supports basic sites. Further studies by Nagaoka et al. [47] using different supports showed that the activity order at pressure of 1 bar was consistent with the basicity of the support.

One of the drawbacks of noble metals is related to their high cost and availability compared to earth abundant transition metals, such as Ni. Improving the stability and the resistance to carbon deposition are of vital importance for developing a commercially viable catalyst for DRM that could be scaled to industrial applications. The properties of noble metals are therefore highly valued, and incorporating them through a bimetallic system appears to be a promising solution. Utilizing noble metals in small amounts as a promoting metal is also considered a more attractive option from an economical point of view.

2.3 Bimetallic Ni Based Catalysts

Bimetallic catalysts have shown promise and has the potential to combine the attributes of different metals. Studies have been conducted by combining other metals with Ni to improve the catalyst for DRM, such as Co, Fe and noble metals. A 5%Co-5%Ni/Al2O3-ZrO2 catalyst improved the surface area and pore distribution in addition to show an increase in active sites after reduction [48]. TGA experiments also showed enhanced resistance to coking for the Co-Ni bimetallic catalyst. Fe-Ni/MgAl2O3 likewise indicated lower carbon deposition on the spent catalyst [49]. In this case it was attributed to the fact that Fe could be oxidized by CO_2 to FeO_x. FeO_x acted as an oxygen carrier and improved the oxidation of the surface carbon from methane decomposition (Eq. 1.6) on Ni particles.

The structure of the bimetallic particles when Ni is modified by other metals, is important to achieve optimum synergetic effect. It seems that the second metal influences the metal particle size and that the added amount is of importance. For example, Ni/α-Al_2O_3 modified by noble metals showed that the noble metals influenced the average metal particle size differently. Increasing the additive amounts of Pd, Rh and Ru lead to an increase in average particle size, while Pt and Ir had the opposite effect [50].

In terms of carbon formation, the effect of Ru loading was studied using a perovskite $LaNi_{1-x}Ru_xO_3$ catalyst [51]. The catalyst with $LaNi_{0.8}Ru_{0.2}O_3$ showed the highest resistance to carbon deposition, although with the drawback of reduced activity. Another aspect is the type of

carbon formed and its reactivity. Carbon formed on the PdNi bimetallic catalyst was found to be more reactive than the carbon formed on the monometallic Ni catalyst [52], which suggests that the addition of Pd alters the structure of the formed carbon. Pt was also found to show this feature through the formation of more reactive intermediate carbonaceous species. This attribute would be advantageous to the catalyst as the activity would remain high despite the carbon deposits and possibly result in more easily removable carbon, which could be beneficial in catalyst regeneration.

Pt, Pd and Rh incorporated to $Ni_{0.03}Mg_{0.97}O$ increased the activity gradually with noble metal loading, reaching a maximum before decreasing with further addition [53]. A drastic improvement in catalytic stability was also found when noble metals were added. The main cause of deactivation was found to be due to oxidation of active Ni species and therefore the increased stability was attributed to enhanced reducibility caused by the noble metals. A different study performed temperature programmed oxidation on a spent NiRh/CeO2-ZrO2 catalyst and the results indicated that there was no direct relation between catalytic activity and amount of surface carbon. Thus deactivation was proposed to be caused partially by oxidation of Ni into NiO and coke formation [54].

The synergy between metal components is of interest, and combining two metals could result in a catalyst with the desired activity and selectivity. Monometallic Rh catalysts shows good stability and decent conversions for DRM, but favors conversion of CH_4 and somewhat relies on the support to achieve high conversions of CO_2. Ni on the other hand has high conversions of both reactants, but is highly susceptible to carbon deposits. In combination Rh and Ni was found to utilize the best of both metals through Ni being more active in the CO_2 conversion, Rh more active in the CH_4 conversion [55] and thereby increasing the overall activity compared to what is achieved by each metal alone. Additionally, the higher carbon deposit resistance of Rh was preserved in the bimetallic catalyst.

Previously, the effects have been described by only focusing on the noble metal content in the bimetallic catalyst. Different studies have used different Ni loading, and it would therefore be beneficial to relate the noble metal content directly to the Ni through a metal/metal ratio. A study on Pt(0.3-0.5 wt%)-Ni(1-12 wt%) bimetallic catalyst showed that the Ni loading should be taken into consideration [56]. The activity of the catalyst was improved by increased Ni loading. However, the carbon deposition was increased at Ni loading over 6 wt%, indicating that the Pt/Ni ratio is important when considering carbon deposition. The promoting effects of the noble metal seem to be present until a point where the behaviors of the Ni particles start to dominate. In the same study [56], both a sequential- and co-incipient wetness catalyst were prepared in order to compare the effect of the preparation method. The catalyst prepared by sequential impregnation was found to have smaller average Ni particle size. This indicates that the bimetallic particles can tailored and that the structure is of importance.

Li et al [57] investigated the structural effects of bimetallic noble-Ni catalysts. Pd-Ni/γ-Al_2O_3 catalysts with similar metal particle size, prepared by the co-impregnation and the sequential impregnation method was used for the analysis. Figure 2.2 shows the proposed model of formation of Ni-Pd particles for both preparation methods, and sequential impregnation results in a higher surface concentration of Pd particles.

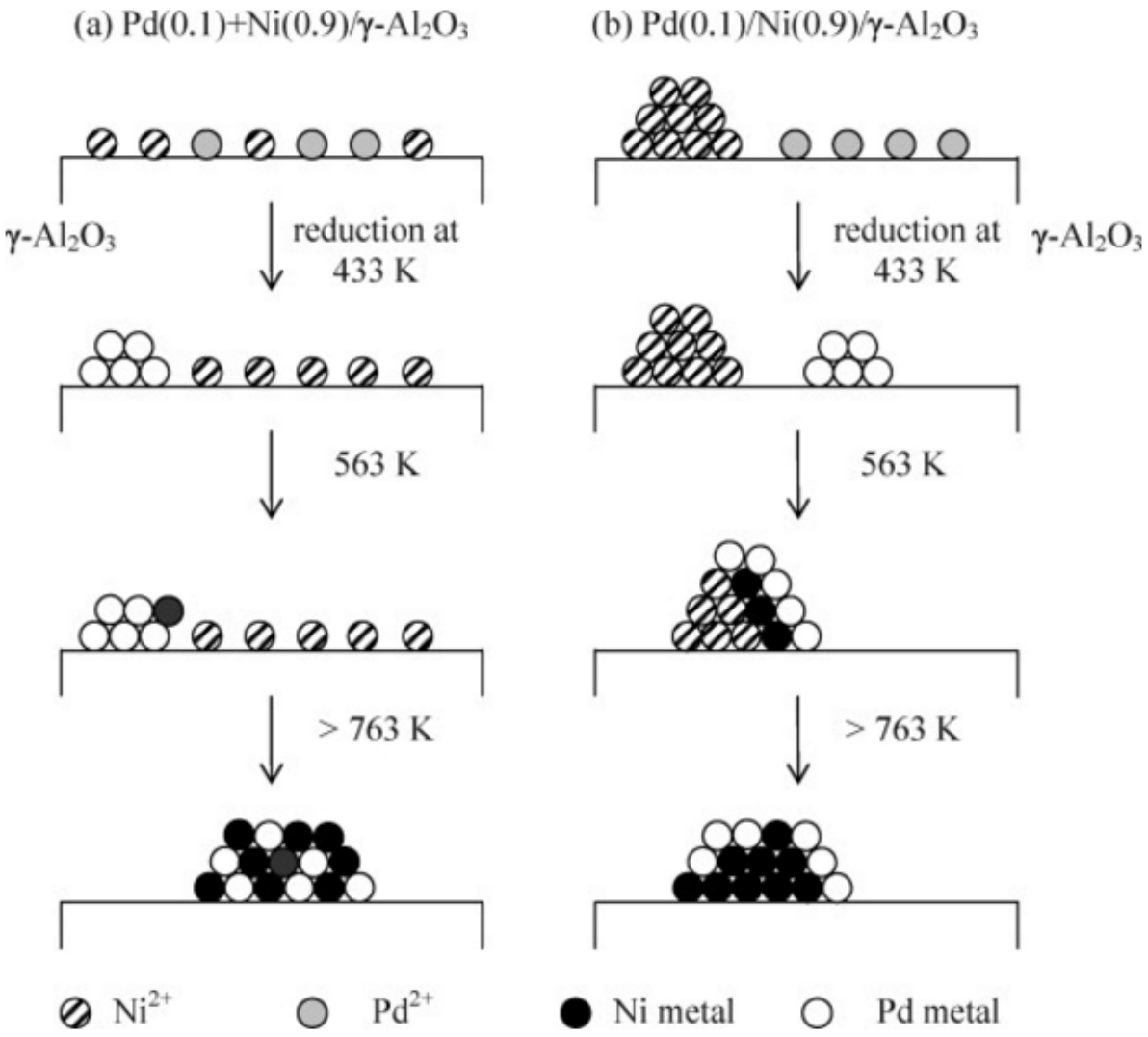

Figure 2.2: Proposed model of the formation mechanism of noble metal-Ni bimetallic particles during the reduction pretreatment: Pd(0.1)+Ni(0.9)/γ-Al2O3 (Co-impregnation) and Pd(0.1)/Ni(0.9)/γ-Al2O3 (Sequential impregnation) *[57]*.

Temperature-programmed reduction revealed that the addition of Pd resulted in a lower reduction temperature, of which the catalyst prepared by sequential impregnation showed the greatest improvement (Figure 2.3). The interaction between the noble metals and the support are not as strong as in the case of Ni, and therefore have a lower reduction temperature. Furthermore, the addition of noble metals weakens the Ni-support interaction and thereby enhances the reducibility of the NiO species. The increased reducibility of the sequential impregnation catalyst can be attributed to the higher amount of Pd particles on the surface.

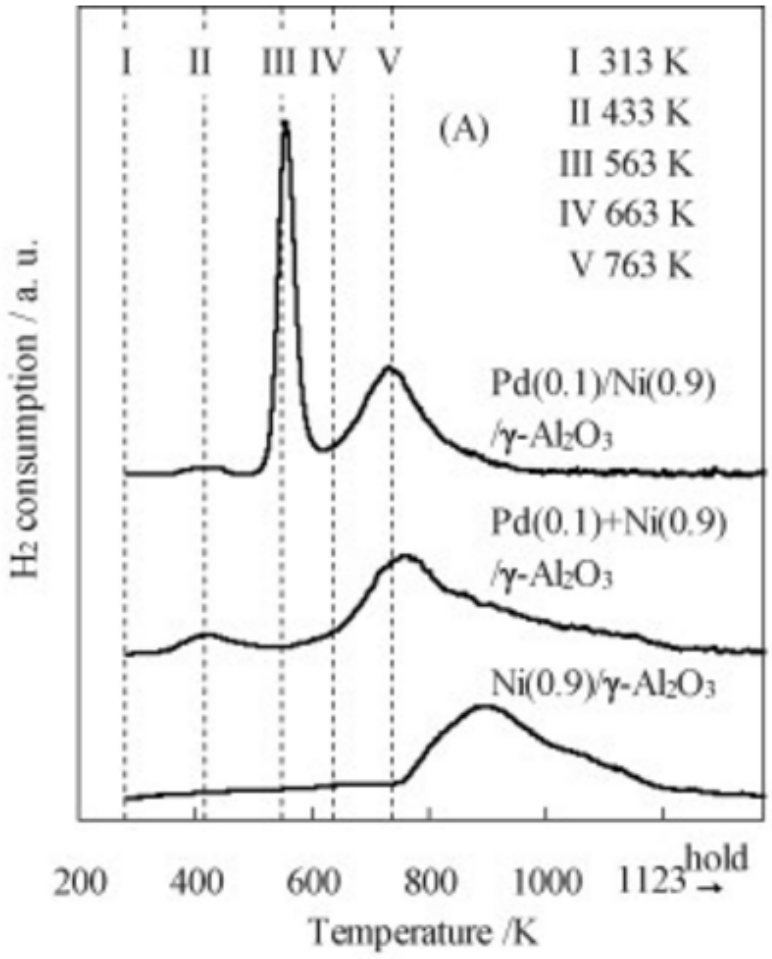

Figure 2.3: Temperature-programmed reduction of Pd-Ni/γ-Al_2O_3 catalysts *[57]*

The same study additionally investigated the surface of the bimetallic Pt(0.2) + Ni(0.9) and Pt(0.2)/Ni(0.9) catalysts by Fourier transform infrared spectroscopy of CO adsorption [57]. It was found that Pt(0.2)/Ni(0.9) showed higher resistance to oxidation. Thus it was concluded that the Pt atoms are located more preferentially on the surface, which can be considered in relation to TPR experiments of Pd/Ni, and indicate an improvement in reducibility.

As Rh, Ru and Ir exhibit a higher stability, one would expect that they would be less mobile during the reduction process in comparison to Pd (Figure 2.2). One study comparing the effect of Pd and Ru with Ni prepared by co-incipient wetness on SiO2 support, showed that the addition of Ru improved the catalyst significantly. On the other hand, the addition of Pd resulted in lower activity and a higher carbon formation rate [58]. The difference was attributed to the bimetallic particle structure, where more of the Pd particles were found to be on the surface. In the case of Ru, it was found that the clusters of Ru were mainly covered by Ni [15, 58, 59], and therefore the formation of small Ru particles led to high Ni dispersion. The result for the Pd modified catalyst appears contradictory to the findings of Li et al [57], which suggested that a higher concentration of Pd at the surface was beneficial. A comparison of the effects of different noble metals can be found in Table 2.2, and it is apparent that there are differences in the findings by different groups.

Table 2.2: List of modified Ni catalyst with noble metals and their effects on the catalyst performance

Catalyst	Noble metal	Noble metal (wt%)	Ni Content (wt%)	Additive effect of noble metal	Ref
M/$Ni_{0.03}Mg_{0.97}O$	Pt, Pd, Rh	0.007-0.032	3	A, S, R	[53, 60]
Rh/Ni/Al_2O_3	Rh	0.05-0.2	10-18	A	[61]
M + Ni/SiO_2	Pd, Ru	0.6	2	Pd: -A, -C Ru: A, S, C, R	[58]
Ru + Ni/SiO_2 **Ru + Ni/ZSM-5**	Ru Ru	0.2-0.6 0.2-0.6	2 2	A(SiO_2>ZSM-5), R, higher dispersion for SiO_2	[59]
Pt/Ni/ZSM-5 **Pt + Ni/ZSM-5**	Pt Pt	0.3-0.5 0.3-0.5	1-12 1-12	A (increased with increasing Ni content), C (Pt's effect reduced over 6% Ni loading, SI>co-I), R	[56]
(0.2-0.4 Ni/Si) Pd/Ni/MCM-41	Pd	0.5	5.4-10.8	A and S: (0.3PdNi>0.4PdNi> 0.2PdNi), R	[52]
$LaNi_{0.95}Rh_{0.05}O_3$ (Sol-gel) **$LaNi_{0.95}Rh_{0.05}O_3$ (co-impregnation)**	Rh Rh	- -	- -	A (particle size smaller for co-impregnation but less thermally stable)	[62]
NiRh/CeO_2-ZrO_2 (Sol-gel)	Rh	0.5	4.5	A, S	[54]
Rh + Ni/α-Al_2O_3	Rh	0.1-1.0	10	A, C	[63]
RhNi/Al_2O_3	Rh	0.1-1.0	10	A, C (Greatest effect at highest Rh loading)	[15]
Pt/Ni/δ-Al_2O_3	Pt	0.2-0.3	10-15	A, C (0.3/10 Pt/Ni highest activity and C-resistance)	[64]
Pt + Ni/nanofibrous γ-Al_2O_3	Pt	0.4-4	10	A, S, C, R	[65, 66]
$LaNi_{1-x}Ru_xO_3$ **x = [0, 0.1, 0.2, 1]**	Ru	-	-	-A , C (highest effect for x=0.2), -R (due to strong Ru – O – La bonds)	[67]
PtNi/nanofibrous γ-Al_2O_3 (Microemulsion method)	Pt	0.4-4	10	A, S, C, R	[68]

M/Ni: Sequential impregnation, M + Ni: Co-impregnation, A: Activity, C: Coke resistance, S: Stability, R: reducibility

It is evident that noble metal incorporation in Ni catalyst can improve the catalytic performance through increasing the activity, improving the reducibility, reducing carbon deposition and improved the stability. For optimal catalytic properties, the amount of noble metal and the

structure of the bimetallic particles should be taken into consideration. The promoting effects exhibited by the noble metals appear to be different to some extent. In addition to the metal-metal synergy, the bimetal-support interaction can affect the catalyst [59], further verifying that the catalyst's performance is down to more than the sum of its parts. From the studies reviewed on bimetallic catalysts it seems clear that the noble metal incorporation is promising, and that further study appears to be required to optimize such a catalyst.

3 Experimental Theory and Procedure

3.1 Theoretical Aspect of Catalyst Synthesis

3.1.1 Incipient Wetness

The incipient wetness method involves a solution of the catalyst precursor (e.g. metal salt) equal (or in proximity) to the total pore volume of the support. The solution containing the active phase(s) is impregnated onto the support structure by filling the pores with the solution. Through controlling the concentration of metal precursor in the solution, the desired active metal loading can be achieved. In contrast to wet impregnation, where the overall loading is limited by e.g. adsorption and/or ion exchange, incipient wetness allows the use of a wide range of metal loading during the deposition process.

The deposition depends on the state of the support material. If in dry state, the deposition process is called capillary- or dry impregnation, the speed of pore filling is fast and the process is simple. However, if the support is already in contact with the solvent (without precursor) the deposition mechanism is known as diffusional impregnation [69].

The last stage is to dry the sample to evaporate the solvent. The drying conditions, as well as the composition of metal components in the system (e.g. monometallic vs. bimetallic), affect the final distribution of the active metal phase(s) [70]. In addition, the distribution profile of the active phase(s) depends on factors related to the solvent (e.g. viscosity), pore size distribution and on the mass transfer conditions within the pores during impregnation and drying [71].

3.1.2 Calcination

Calcination is the high-temperature treatment of prepared catalyst in air or inert atmosphere. The precursors used to synthesize the catalyst might result in hydroxides, nitrates or carbonates, which are not desired in the final catalyst. The purpose is to decompose and volatilize the various catalyst precursors formed in the preparation and thereby remove impurities and unwanted compositions from the catalyst, in addition to stabilize physical and chemical properties of the catalyst [72].

Changes to the pore structure and the formation of new compounds can occur during calcination, and depends on the metal components in the system, calcination atmosphere, temperature and duration [73]. Furthermore, amorphous material can become crystalline. In case of γ-Al2O3, the surface area and pore volume has been shown to decrease with increasing calcination temperature. In addition, for nickel based catalysts the nickel dispersion, the nickel surface area and the reducibility decreased with increasing calcination temperature. The most stable catalyst was obtained at a calcination temperature of 700 ^{o}C [74]. The study indicated that the calcination can have significant effects on the catalyst performance.

3.1.3 Activation

Reduction is the final treatment in the production of catalysts and the purpose is to convert metal oxides into active metals by the use of a reducing agent, such as H_2. The temperature is a crucial parameter in the reduction process and can affect the dispersion, the surface area and the extent

of reduction for the metal-support system. The heating rate and hydrogen space velocity can also have an impact on the surface area and the degree of reduction of the catalyst [72]. The optimal reduction temperature is different and depends on the components of the catalyst.

3.2 Theoretical aspect of catalyst characterization

3.2.1 X-ray Diffraction

X-ray diffraction can be used to characterize crystalline materials and determine their structure. Each crystalline solid has its own unique characteristic X-ray pattern, which is used to identify the phase. The X-ray diffractometer consist of three basic elements: An X-ray tube, a sample holder and an X-ray detector. A metal is used as the source of the X-rays and is referred to as the target metal. The wavelength of the produced X-rays depends on the target metal and most commonly Cu (λ=1.5418 Å) and Mo (0.7107 Å) is used. The d-spacings that can be observed depends on the wavelength through d = λ/2, and thus sets a limit to the size of the crystallites that can be observed.

The produced X-rays are collimated and directed towards the sample. The intensity of the reflected X-rays is recorded as the sample is rotated in the desired range (typically 5^o to 70^o). When the geometry of the incident X-rays impinging the sample satisfies the Bragg Equation (Eq. 3.1), constructive interference occurs and a peak in intensity arises [75].

$$2dsin\theta = n\lambda \qquad \text{(Eq. 3.1)}$$

Where d: d-spacing, θ: Bragg angle, λ: X-ray wavelength, n: a positive integer

The position of the peaks in the X-ray pattern is used to determine the type of crystalline structure that is present in the sample. One approach is to do cross matching with a database containing information about the d-spacings of known minerals. The Scherrer equation (Eq. 3.2.) can be used to find an approximate value of the particle size of crystallites.

$$d_c = \frac{k\lambda}{\beta cos\theta} \qquad \text{(Eq. 3.2)}$$

Where d_c: average crystalline size, K: dimensionless shape factor depending on the actual shape of the crystallite, λ: X-ray wavelength, β: line broadening at half of the maximum intensity, θ: Bragg angle

3.2.2 Textural Measurements

Surface area, pore volume and pore diameter can be investigated through the Brunauer Emmett Teller (BET) method and Barrett-Joyner-Halenda (BJH) method. Known amounts of nitrogen gas are released stepwise into the sample cell, where nitrogen adsorption onto the surface takes place. The interaction between gaseous and solid phases is usually weak and therefore the surface is cooled using liquid N_2 to obtain detectable amounts of adsorption. Relative pressures lower than atmospheric pressure is used in each step. The saturation pressure can be determined by further increasing the pressure until no more adsorption occurs, regardless of pressure increase. After adsorption the nitrogen is released from the material through heating and quantified. The collected data is presented in the form of an isotherm, which plots the amount of

gas adsorbed as a function of the relative pressure. Multiple points (normally in the range 0.05 to 0.3 relative pressure) or single point (intercepting the line with 0) can be used to determine the surface area of the sample. The BET method [76] is applicable at low relative pressures and is written in the linear form:

$$\frac{p}{n_a(p_o-p)} = \frac{1}{n_{a.m}C} + \left(\frac{C-1}{n_{a,m}C}\right) p/p_o \qquad \text{(Eq. 3.3)}$$

Where p: sample pressure, p_o: saturation vapor pressure, n_a: amount of gas adsorbed at the relative pressure p/p_o, $n_{a,m}$: the monolayer capacity, C: BET constant

From the adsorption and desorption isotherm, pore size and pore volume can be determined by BJH method [77].

3.2.3 **Dispersion**

There are several methods for determining the dispersion of active metals, and the static volumetric method is one of them. It involves supplying an adsorbing gas (e.g. H_2) into a determined volume containing the sample. To determine the volumes and quantities of gas accurately, it is required to quantify all volumetric spaces and temperatures within the system. The gas adsorbed is then determined by the difference between the total amount of gas and the gas remaining in the free space of the system. A Langmuir adsorption isotherm is created by utilizing ultra-low-pressures and a stepwise increase in total pressure while determining the quantity adsorbed at each pressure level.

A pressure level will first yield an adsorbed amount consisting of both physisorption and chemisorption. To differentiate the chemisorption from the contribution of physisorption, the sample is evacuated after completion of the initial analysis, which removes only the reversibly adsorbed gas. Next, the analysis is repeated under the same conditions as the original analysis and now the active area is already saturated with chemisorbed molecules. Thus, the chemisorbed amount can be determined by subtracting the initial total adsorbed gas by the reversible adsorbed gas in the following analysis. Figure 3.1 illustrates the development of the chemisorption isotherm [78].

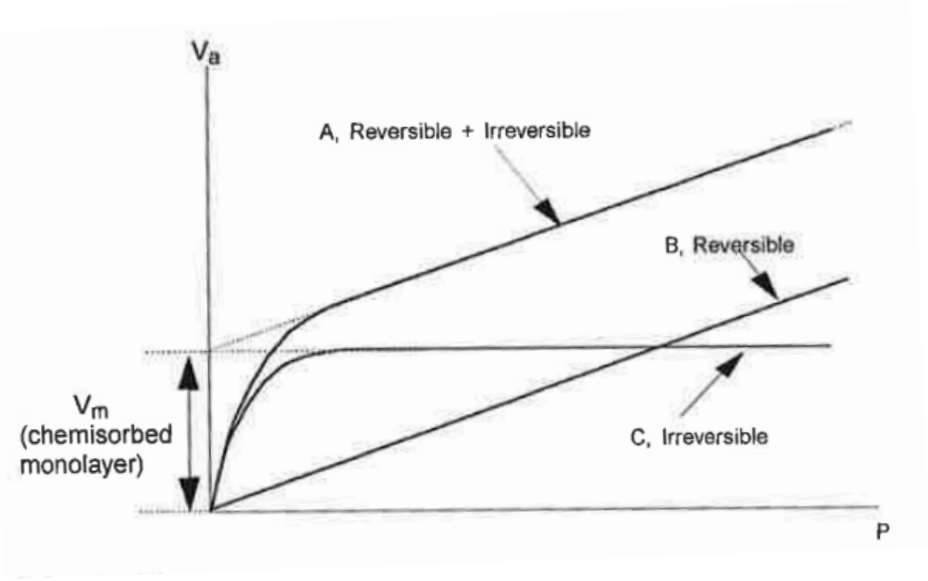

Figure 3.1: Isotherms generated by the technique of volumetric chemisorption. A: Chemisorbed + Physisorbed, B: Physisorbed, C: Chemisorbed (Langmuir-type isotherm) *[78]*

Through the Langmuir model the active sites on the surface, N_s, can be determined from the isotherm by the relationship:

$$N_s = \frac{V_m N_A F_S}{V_{mol}} \qquad \text{(Eq. 3.4)}$$

Where V_m: monolayer volume obtained by static volumetric technique, N_A: Avogadro's number, Fs: stoichiometry factor depending on adsorptive (e.g. 2 for H_2 on Ni and Pt), V_{mol}: molar volume of the adsorptive.

The fraction of the total active metal, N_T, accessible to the reactant molecules is called the dispersion γ(%) (Eq. 3.5).

$$\Upsilon\% = \frac{N_S}{N_T} * 100 \qquad \text{(Eq. 3.5)}$$

The active metal particle size can be estimated, but requires an approximation by assuming the particle geometry. In the case of spherical geometry, the particle diameter can be calculated by the following relationship:

$$d = \frac{6}{(A_{Sm})(\Upsilon\%)(\rho)} * 100 \qquad \text{(Eq. 3.6)}$$

Where A_{Sm}: active area per gram of pure metal, ρ: density of the metal, 6 results from the area-to-volume ratio for a sphere (A/V = 6/d).

The active metal area is that portion of the total metal located on the surface of particles which are accessible to the adsorption gas and can be calculated by the formula:

$$A_m(m^2/g) = F_S n_a N_A A_g \qquad \text{(Eq. 3.7)}$$

Where n_a: number of moles of gas adsorbed cm^3/g STP determined at the monolayer, A_g: the cross-sectional area of the active adsorptive atom.

3.2.4 **Temperature Programmed Reduction**

The temperature programmed reduction (TPR) method yields quantitative information of the reducibility of the metal oxide's surface, as well as the heterogeneity of the reducible surface. It can determine the number of reducible species present in the catalyst and reveal the temperature at which the reduction occurs. This information can be used to find the optimal reduction conditions and to determine the role of second components (e.g. bimetallic catalyst).

The technique of TPR is to subject a catalyst to a programmed temperature rise, while a reducing gas mixture is flowed over it. The reducing reaction between a metal oxide (M_xO_y) and hydrogen (Eq. 3.7) produces a pure metal M and results in a lower concentration of H_2 in the gas mixture. The reduction rate is continuously monitored by measuring the change in composition of the reactive mixture exiting the reactor by thermal conductivity [79].

$$M_xO_{y\,(solid)} + H_2 \rightarrow M_{(solid)} + H_2O \qquad \text{(Eq. 3.7)}$$

From a thermodynamic point of view, the reduction of a solid oxide is feasible if the Gibbs free energy is negative (Eq. 3.8), and thus depends on the metal species and their interaction with the catalytic system. Thereby it is also possible to give an indication of, or possibly identify, different metal species present in the catalyst.

$$\Delta G = \Delta G^0 + RTlog(\frac{P_{H_2O}}{P_{H_2}}) \qquad \text{(Eq. 3.8)}$$

During the TPR analyses it is necessary to remove the produced water that is formed, as the water can interfere with the measurement. In addition, it has been reported that the experimental conditions affect the temperature at which the reduction occurs [80].

It is possible to quantitatively calculate the amount of reduced sites, and the reduction rate can be expressed by the equation:

$$r = -\frac{d[M_xO_y]}{dt} = -\frac{d[H_2]}{dt} = k[M_xO_y]^p[H_2]^q \qquad \text{(Eq. 3.9)}$$

Where k is a constant given by the Arrhenius equation $k=Ae^{-E/RT}$ *and* $dT = \beta\, dt$*, T is the temperature (K) and t is time (min).*

As the temperature is increased linearly, it is possible to correlate the concentration variation of the reactive gas by:

$$\frac{d[H_2]}{dt} = -\frac{\beta d[H_2]}{dT} \qquad \text{(Eq. 3.10)}$$

The TPR data offers information about the rate of change for certain parameters as a function of temperature. By correlating reduction profiles to kinetic/thermodynamic parameters, the consumption rate of the reactive gas *r*, is correlated to the flowrate *φ*, to the reactor element *dx* and the fraction of conversion *df* by the following expression:

$$r = \varphi \frac{df}{dx} \qquad \text{(Eq. 3.11)}$$

3.3 Catalyst Synthesis Procedure

The supports used in synthesizing the catalyst were Puralox Th 100/150 γ-Al2O3 and Puralox SCCa-5/200 γ-Al2O3, both produced by SASOL. The active metal precursors used were purchased from Sigma-Aldrich and can be found in Appendix A.

3.3.1 Pore Volume Measurement

In order to measure the pore volume of each support, deionized water was gradually added to 5 grams of support until water was detected on the support surface. The fact that water cannot be absorbed anymore by the support, means that the pores are saturated. This procedure was repeated three times to ensure that the proper pore volume was determined, and the results were averaged. The point of saturation is determined by observation and thus is influenced by personal experiences. The pore volume per gram of support was calculated by the following relation:

$$\text{Pore volume} = \frac{\text{Amount of water for saturation (ml)}}{\text{Weight of support (g)}} \qquad \text{Eq. 3.12}$$

Table 3.1 shows the support specifications from the datasheet and the averaged pore volume determined from the experiments.

Table 3.1: Support specifications

Support	Pore Volume Datasheet	Loose bulk Density g/ml	Particle Size distribution	Determined pore volume
Th 100/150	1,062 ml/g	0.36	<25 μm – 41.2% <45 μm – 71.7% <90 μm – 97.7%	1.683 ml/g
SCCa-5/200	Not disclosed	0.75	<90 μm – 74.6% <125 μm – 95.8%	1.036 ml/g

The two supports had different densities. After impregnation the Th 100/150 yielded about twice the amount in volume compared to SCCa-5/200. The determined pore volume was also high compared to the datasheet. The pore volume listed in the datasheet is probably determined by BET measurements.

3.3.2 Incipient Wetness

Catalyst synthesis was done according to incipient wetness method. A weighed quantity of support was used as the basis to calculate the required amount of active metal precursor(s) to achieve the desired metal loading. The crystal water in the Ni precursor was subtracted from the total pore volume of the weighed support, in order to determine the accurate water amount to be added. The calculated amount of water was then added to the glassware and marked before removing the water and drying the glassware. Calculated amount of active metal precursor was added to the dried glassware and then mixed with deionized water until the marked volume was reached. Stirring of the mixture was performed to ensure that the precursor(s) was fully dissolved and heat was applied if needed. Finally, the solution was added dropwise to the support and distributed into the pores using a pallet and mortar. Drying of the synthesized catalysts was done in air at 80 ^{o}C for 12 hours. Table 3.2 below shows the series of catalysts that have been synthesized, with the metal loadings of Ni and precious metals.

Table 3.2: List of synthesized catalysts in this work

Metal loading [wt %]					Support	Designation
Ni	Pt	Pd	Rh	Ru		
12	0	0	0	0	Th-150/5	Ni/Th
12	0	0	0	0	SCCa/200-250	Ni/SCCa
12	0.5	0	0	0	SCCa/200-250	PtNi/SCCa
12	0	0.5	0	0	SCCa/200-250	PdNi/SCCa
12	0	0	0.5	0	SCCa/200-250	RhNi/SCCa
12	0	0	0	0.5	SCCa/200-250	RuNi/SCCa

3.3.3 Calcination

All the as-prepared catalyst were calcined in air in a Nabertherm P330 muffle furnace. Each catalyst was loaded into a crucible that was placed inside the furnace at room temperature. The temperature was increased by 2 ^{o}C/min up to 600 ^{o}C and then kept at 600 ^{o}C for 6 hours before gradually being cooled to room temperature. After calcination the catalyst was crushed with a pallet and mortar.

The effect of static air could result in a lower transportation of impurities and water vapor from the catalyst. It should therefore be noted that the calcination was not done at optimal conditions due to lack of necessary equipment.

3.4 Catalyst Characterization Procedure

3.4.1 X-ray Diffraction

X-ray diffraction patterns were recorded for calcined catalysts at room temperature by a Siemens D500 X-ray diffractometer using CuKα radiation (λ = 1.5418 Å). The analysis was performed from 10^{o} to 100^{o} with a step size of 0.030^{o}/min. The divergence slit was set at 1^{o} and the diffractometer. The peaks were identified by comparison with standards in a database.

3.4.2 Textural Measurements

BET surface area, pore volume and average pore diameter of the synthesized catalysts were measured using Tristar II 3020 (Micromeritics) by adsorbing N_2 at its liquefaction temperature of 77 K. Prior to the N_2 adsorption process, the catalysts were degassed at 120 ^{o}C for 5 hours. About 0.2 g of catalyst was used for each measurement. All the runs were performed with 6 adsorption points (0.05 – 0.3 relative pressure).

3.4.3 Dispersion

The active metal dispersion and particle size was measured by Chemisorption (ASAP 2020 Plus, Micromeritics). The sample was placed in a quartz u-tube and held in place by a quartz wool plug. About 0.2 g of catalyst was used for each measurement. First, the sample was pretreated to dry the sample and remove impurities with He flow while the temperature was ramped from ambient to 200 ^{o}C at a rate of 25 ^{o}C/min. Then the sample was heated to 600 ^{o}C at 10 ^{o}C/min with flow of

H_2. After reducing the catalyst for 30 minutes at 600 ^oC, the sample was cooled to 35 ^oC at a rate of 10 ^oC/min. After pretreatment, the chemisorption isotherm was determined as described in 3.2.3 by using 13 pressure points below atmospheric pressure, yielding the active metal dispersion and particle size.

3.4.4 Temperature Programmed Reduction of Catalyst

Temperature programmed reduction (TPR) of the catalysts were performed in an AutoChem II 2920 (Micromeritics) fixed bed reactor. About 30 mg of catalyst was loaded in a 6 mm inner diameter (ID) quartz u-tube. The catalyst was held in place by a quartz wool plug. A thermocouple was inserted approximately 1 mm above the catalyst bed and ran axially through the quartz reactor, in order to measure and control the bed temperature. The temperature was ramped from ambient to 950 ^oC at a rate of 10 ^oC/min while flowing 10% H2/Ar at 50 ml/min over the catalyst. After the measurement, the amount of H_2 consumed, which is quantified by a TCD detector signal, was plotted as a function of temperature.

3.5 Dry Reforming of Methane

3.5.1 Calibration of the Gas Chromatogram (GC) column

The GC was used to analyze the effluent gases resulting from the DRM reactions. The GC was calibrated to find the response time of the different compounds. The main products in DRM are H_2, CO, CH_4, CO_2 and relatively small amounts of H_2O. H_2O is removed from the gas before measuring. Byproducts formed in the reaction are in very low concentration and has therefore been neglected [81]. Calibration was done using a calibration gas containing 5% Propylene, 5% Ethylene, 5% N_2, 20% CO_2, 20% CO, 20% H_2 and 25% CH_4.

3.5.2 Experimental Setup

A schematic of the experimental setup can be found in Figure 3.2. The feed units consist of four gas feed lines for N_2, CH_4, H_2 and CO_2, each having a manual pressure regulation valve set to 5 bar. Following, is the mass-flow controllers (Alicat) which regulates the flowrate of each gas according to the set flowrate. In front of the reactor is a safety pressure relief valve in order to avoid pressure buildup in the reactor. A pressure gauge is also installed prior to the reactor to monitor the pressure. The reactor is a stainless steel tube with a 1/2" internal diameter, and heating is done by an electrical oven surrounding the reactor controlled by a temperature regulator (Eurotherm 3280). The temperature was measured by a K-type thermocouple positioned axially inside the reactor. To position the catalyst bed just below the thermocouple, a stainless steel tube with internal diameter of 9mm was placed in the bottom of the reactor. The gasses are preheated before entering the reactor by passing through the oven. A pressure relief valve and a pressure gouge are also installed after the reactor. The gas mixture then passes through a coalescing filter to remove water from the gas. A pressure controller (Alicat) is used to maintain the reaction pressure at 1 atm. To ensure a stable flowrate to the GC, a splitter is used and the gasses were vented after measurement.

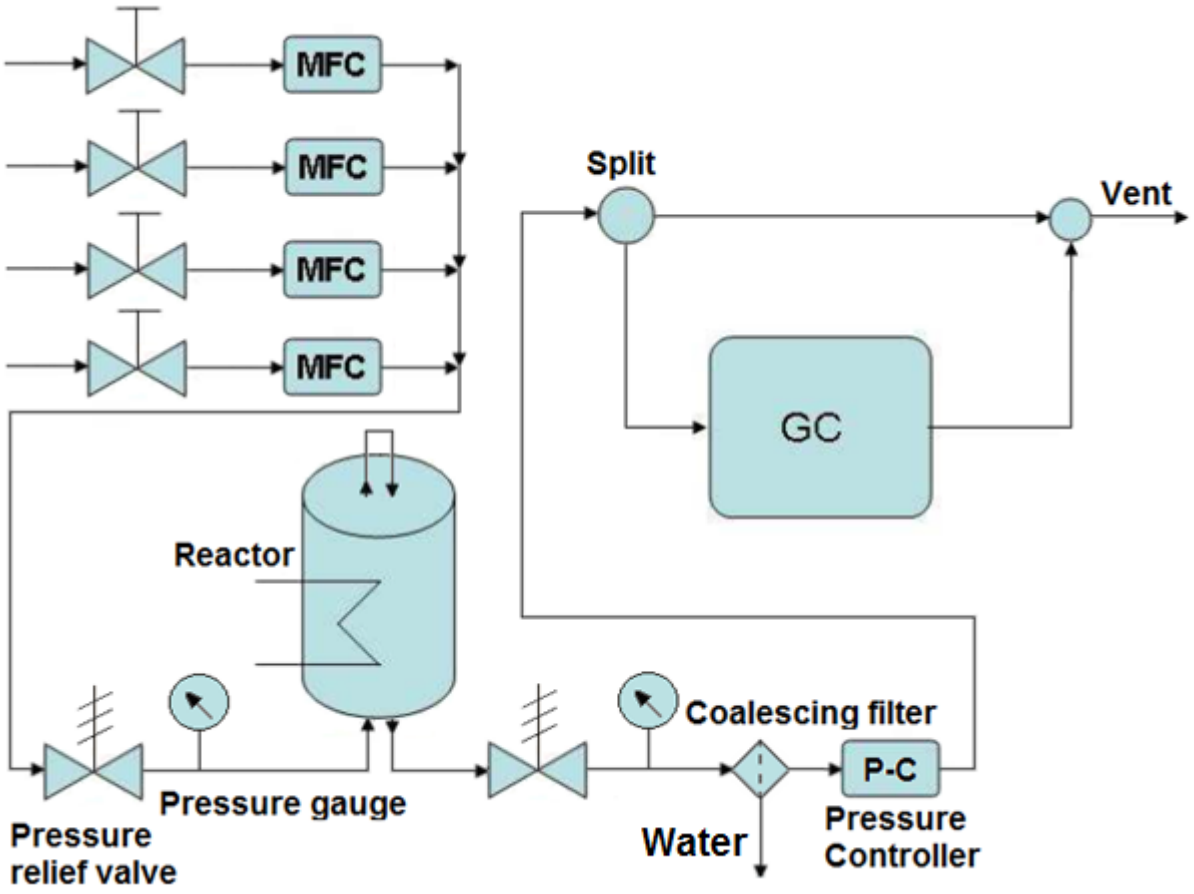

Figure 3.2: Schematic of the experimental setup

3.5.3 Experimental Procedure

For each run, 50 mg of catalyst was measured and mixed with SCCa at a ratio of 1:10 to avoid hot spots in the catalyst bed and dilute the catalyst to reduce the risk of blockage. A quartz plug was placed on top of the 9mm stainless steel tube in the bottom of the reactor and then the diluted catalyst was added. The reactor was heated to 600 ^{o}C at a rate of 5 ^{o}C/min with a flowrate of 50 Scm^3/min of N_2. Reduction was done at 600 ^{o}C for 6h with 50% H_2 and 50% N_2 at a combined flowrate of 100 Scm^3/min. After reduction, the temperature was increased to 700 ^{o}C with N_2 at a flowrate of 50 Scm^3/min. The DRM reaction was carried out with a 1:1 ratio of CH_4/CO_2 with a total flowrate of 100 Scm^3/min, resulting in a GHSV of 120 000 Scm^3 g_{cat}^{-1} h^{-1}. The pressure was maintained at 1 atm throughout the process. The activity was measured after ensuring steady state (usually after 10 minutes from reaction initiation over the catalyst). All the gases were 99.99% pure and supplied by Yara Praxair. Catalyst stability was monitored continuously with time on stream (TOS 15h). Concentration of the effluent gases from the reactor was determined using an online GC (Agilent 7890B, thermal conductivity detector). Reactant conversions and yields was determined by Eq. 3.13-3.16.

$$X_{CH4}\% = \frac{C_{CH4,in} - C_{CH4,out}}{C_{CH4.in}} * 100 \qquad \text{(Eq. 3.13)}$$

$$X_{CO2}\% = \frac{C_{CO2,in} - C_{CO2,out}}{C_{CO2.in}} * 100 \quad \text{(Eq. 3.14)}$$

$$Y_{H2}\% = \frac{C_{H2,out}}{2C_{CH4.in}} * 100 \quad \text{(Eq. 3.15)}$$

$$Y_{CO}\% = \frac{C_{CO,out}}{C_{CH4,in} + C_{CO2,in}} * 100 \quad \text{(Eq. 3.16)}$$

Where X_i and Y_i are the conversion of reactants and yield of products respectively, $C_{i,in}$ is the initial molar fraction of component i in the feed and $C_{i,out}$ is the final molar fraction of component i in the product stream [82].

4 Results and Discussion

4.1 X-Ray Diffraction

The spectrum of γ-Al_2O_3 is known to have a spinel structure where Ni can occupy the tetrahedral or octahedral sites in the structure. This leads to a decrease in the cationic deficiency of γ-Al_2O_3 thus stabilizing the structure [83]. The XRD spectrums of the supports, with and without calcination, and the nickel catalysts are shown in Figure 4.1. The increase in the peak observed at 45,9º and 66,9º for the calcined support is attributed to changes to the support during calcination that lead to a higher degree of crystallization.

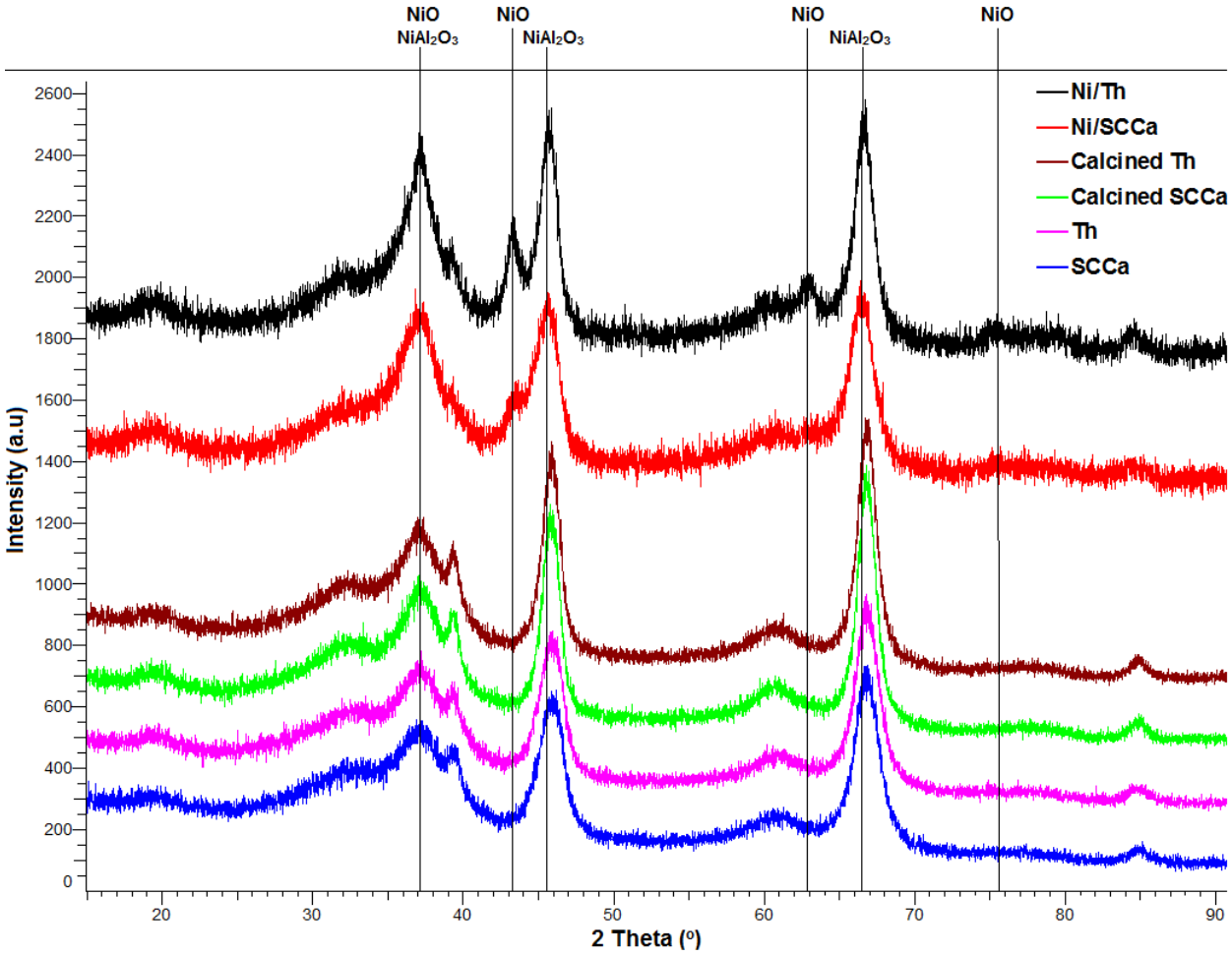

Figure 4.1: X-ray diffraction spectra of the supports before calcination, and supports and monometallic nickel catalysts calcined at 600 ºC

Nickel alumina spinel has an onset temperature during calcination temperature above 500 ºC [84] and it can be expected that it will be present in the catalysts. Stoichiometric nickel alumina spinel ($NiAl_2O_3$) has a peak at 45.0º and 65.5º. The shift of the diffraction peaks relative to the peaks at 45,9º and 66,9º indicates that there are nickel alumina spinel species in both catalysts. A slightly higher shift is observed for the Ni/SCCa catalyst, which could correspond to a higher degree of

crystallinity for the nickel alumina spinel. $NiAl_2O_3$ has a characteristic peak at 37º and therefore effects the peak at 37.1º.

The Ni based catalysts showed characteristic peaks at 43,3º, 62,9º and 75,4º for NiO. In addition, NiO crystallites affects the peak at 37º due to its characteristic peak at 37,3º. A slight shift was also observed for this peak for Ni/Th. The crystallite size can be calculated by the Sherrer equation (Eq. 3.2), and width of the peak at half maximum is inversely proportional to the crystallite size. The peak at 43.3º is slightly broader for Ni/Th, which corresponds to larger crystallite size.

A comparison of the catalysts containing noble metals to the Ni/SCCa catalyst is shown in Figure 4.2. XRD can typically only detect metal crystallites that are larger than 2-5 nm [85]. The noble metals were not detected as oxides or alloys for any of the noble metal modified catalysts. This is to be expected due to their low concentration. The clusters of noble metals present in the catalysts are likely to have small particle size and be well dispersed.

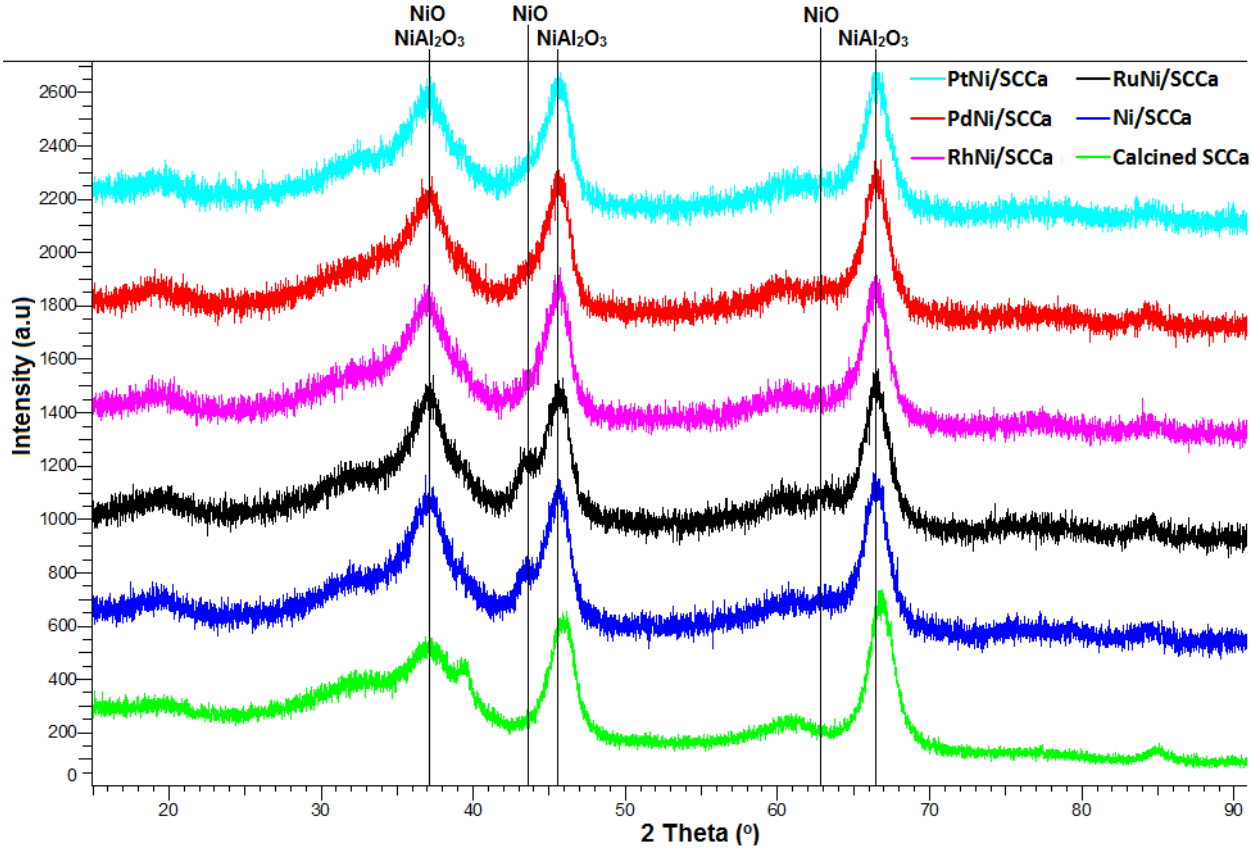

Figure 4.2: X-ray diffraction spectrums of Ni/SCCa and noble metal (Pt, Pd, Rh, Ru) modified Ni/SCCa. The calcined support is shown at the bottom for reference.

Nickel alumina spinel were detected for all the noble metal catalysts. The RuNi/SCCa catalyst had a clear peak corresponding to NiO at 43.3º, and a slight increase in intensity was also observed for the other noble metal catalyst. At 62,9º, both PdNi/SCCa and RuNi/SCCa had a small peak due to NiO crystallites. Odriozola et al. found that the co-impregnated Ru(0.4 wt%)-Ni(15.2 wt%) catalyst showed a reduction in NiO particle size in the XRD spectra [86]. From the

XRD spectra, it does not appear clear if Ru influenced the nickel particles size in the catalyst investigated in this thesis.

The stabilizing effect of noble metals in the bimetallic particles could result in a lower degree of NiO crystallization at the calcination temperature used in this work (600 ^{o}C). Therefore, it is possible that it resulted in a higher degree of NiO remaining amorphous.

4.2 Textural Results

Nitrogen adsorption isotherm at relative pressure 0.05 to 0.3 for the catalysts can be found Figure 4.2. The isotherms indicate that the catalysts have similar textural properties, although the adsorbed amount of N_2 is decreasing with metal loading. Pt and Pd show almost identical isotherms while Ru and particularly Rh reduces the amount of N_2 adsorbed even further.

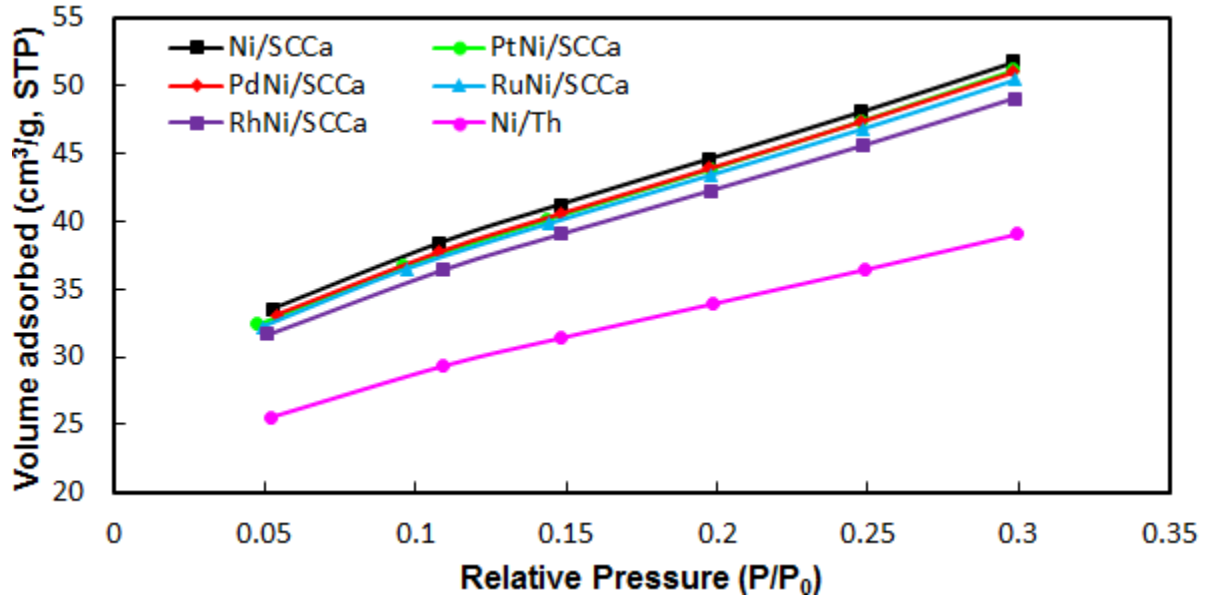

Figure 4.3: Nitrogen adsorption isotherms at relative pressure 0.05-0.30 P/P_0.

The range investigated is sufficient for measuring the surface area through the BET method. However, as the Langmuir adsorption isotherm and the desorption isotherm were not determined, the BHJ method will not yield the correct pore volume and average pore diameter. For illustrative purposes, a typical isotherm for γ-Al_2O_3 is shown in Figure 4.4.

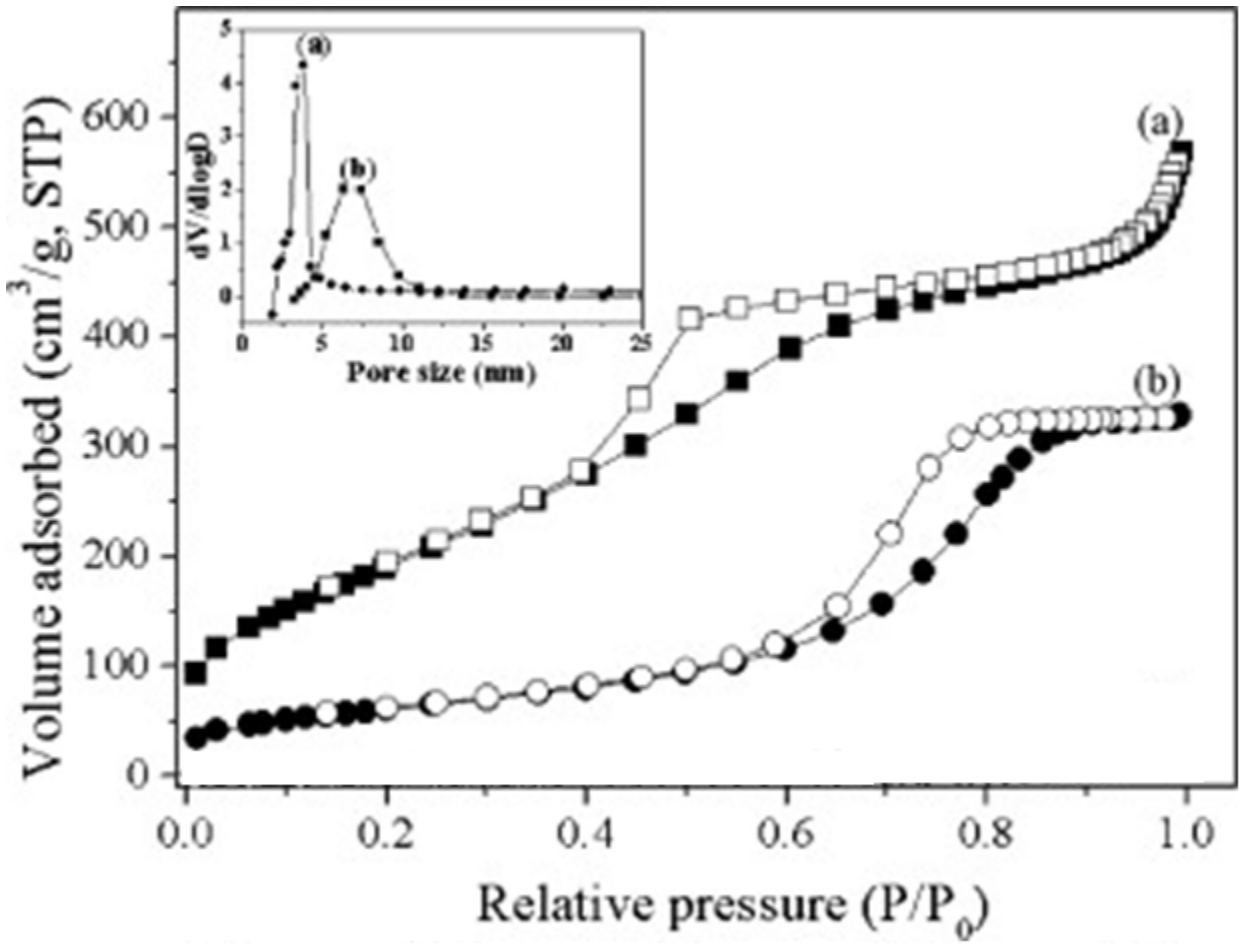

Figure 4.4: N_2 adsorption-desorption isotherm and pore size distribution: (a) Mesoporous alumina with surface area 812 m^2/g, pore volume 0.83 cm^3/g and narrow pore size distribution, (b) commercial γ-Al2O3 with surface area 220 m^2/g and pore volume 0.54 cm^3/g *[87]*.

Table 4.1 shows the averaged results obtained from textural measurements for the surface area and the results obtained from the BJH method. It can clearly be seen that the pore volume and average pore diameter is very low. Comparing the values to the commercial γ-AL_2O_3 in Figure 4.4, it is clear that the BJH method is not suitable at the pressure range used in the experiments for the catalysts investigated in this thesis.

Comparing the initial state support to the calcined support, it is apparent that the support was highly stable at the calcination temperature of 600 ^oC. Others have reported that nickel particles plugs the pores of the support, which leads to a lower surface area [56]. In addition, the surface area was found to be reduced with increasing metal loading. In our case, the surface area decreased with the modification of noble metals. The lowest surface area was found for Rh and Ru modified catalysts.

Table 4.1: Physical analysis results for supports and calcined catalysts

Catalyst	BET surface area[3] (m2/g)	Total Pore Volume[3] (cm^3/g)	Average pore diameter[3] (nm)	Metal loading[4] (weight %)
y-Al2O3 (Th)[1]	142.13 (150[3])	0.092	2.16	-
y-Al2O3 (Th)[2]	140.89	0.092	2.21	-
y-Al2O3 (SCCa)[1]	192.28 (206 [3])	0.124.	2.20	-
y-Al2O3 (SCCa)[2]	184.78	0.118	2.13	-
12Ni/Th	121.35	0.807	2.26	12
12Ni/SCCa	162.11	0.106	2.24	12
0.5Pt12Ni/SCCa	160.10	0.104	2.25	12.5
0.5Pd12Ni/SCCa	158.98	0.104	2.27	12.5
0.5Rh12Ni/SCCa	152.95	0.101	2.25	12.5
0.5Ru12Ni/SCCa	153.80	0.102	2.21	12.5

1: Support before calcination
2: Support after calcination
3: Determined from textural measurements
4: Calculated theoretical value

The two supports used was found to have a significant difference in surface area. All the SCCa supported catalysts have similar surface area, and it is expected that the small additional reduction in surface area for the Rh and Ru modified catalysts will not significantly affect their performance.

4.3 Dispersion

Figure 4.3 illustrates how inaccessible metal species will affect the results obtained in the dispersion experiment. The amount of active molecules accessible to the gas is of importance as the dispersion is related to the available surface area. An increased amount of active molecules would be lost inside the bulk if the particle size increases. Additionally, the inaccessible metal will also decrease the dispersion. Thus the dispersion obtained for the monometallic Ni catalysts at 600 ^oC will give an indication of the available active metal in the DRM experiments in this work. The results obtained for dispersion, particle size and active metal surface area is presented in Table 4.2.

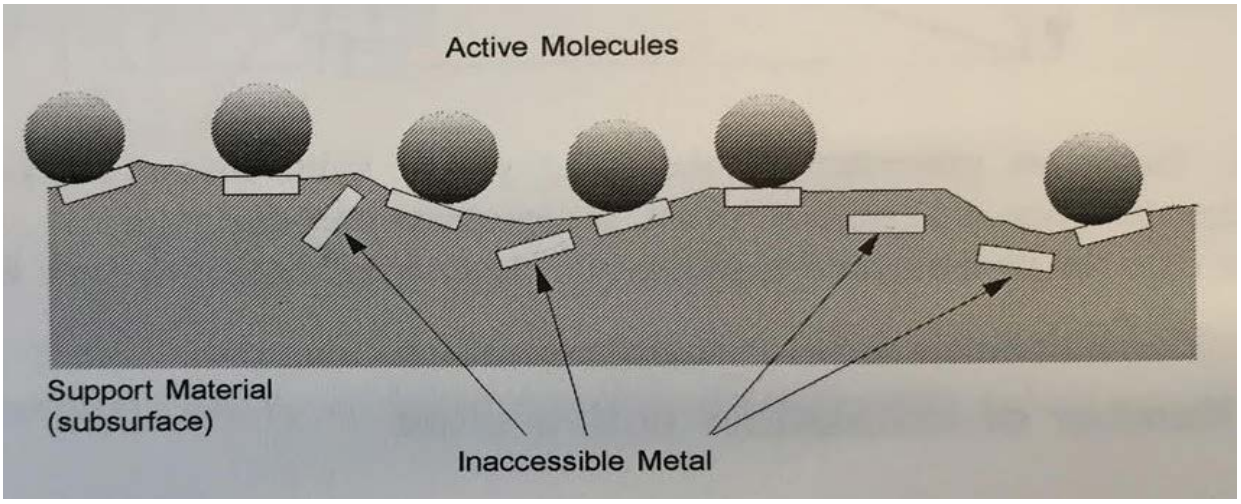

Figure 4.5: Illustration of active metal dispersion

The catalysts were prepared by the same procedure. The calcination temperature is proposed to have the largest effect on particle redistribution, thus differences in the impregnation process is considered to have less of an impact. In regards to the large difference in the results, it is most likely related to the support for monometallic Ni catalysts. One possibility is a higher stability of NiO particles deposited on the Th support, thus resulting in a lower amount of Ni migration and development of nickel spinel species. The development of nickel alumina spinel stabilized the support structure and results in highly dispersed Ni particles. The remaining NiO species might therefore be present as smaller particles, and the increase in crystallite size observed is due to nickel alumina spinel not being reduced in the pretreatment. It could also be related to the other properties of the support structure, such as the amount of tetrahedral and octahedral sites.

Table 4.2: Dispersion results obtained by chemisorption

Catalyst	Dispersion (%)	Crystallite size (hemisphere) (nm)	Metallic area (m^2/g metal)	Temperature of reduction in pretreatment
Ni/Th	4.2794	23,66	28.4883	600 ^oC
Ni/SCCa	2.3777	42.58	15.8288	600 ^oC
Ni/Th	2.3335	202.46	3.3290	400 ^oC
Ni/SCCa	0.3706	273.21	1.2301	400 ^oC
PtNi/SCCa	3.5746	28.56	23.1977	400 ^oC
PdNi/SCCa	0.2248	452.92	1.4765	400 ^oC
RhNi/SCCa	2.5285	40.22	16.6042	400 ^oC
RuNi/SCCa	0.2723	373.85	1.7888	400 ^oC

The dispersion and the crystallite size is calculated based on the amount of active metals that are present in the sample. Based on the TPR data there appears to be a significant amount of nickel alumina spinel in all the catalyst, both the dispersion and crystallite size will therefore not be directly representative for the NiO species on the support surface. The TPR results could be used to calculate the amount of reduced Ni species at 600 ^{o}C and thus be used for correction for the crystallite size. This has not been done in this work but the difference in reducibility is large. Thus, a visual estimate will be sufficient to assess the crystallite size obtained from the dispersion.

The reduction temperature used before initiating the DRM reactions was 600 ^{o}C, which will generally not reduce the nickel alumina spinel and thus the important nickel species contributing in the DRM reactions in this work are mainly NiO.

4.4 Temperature Programmed Reduction

4.4.1 Experimental Considerations

The TPR experiment was run without pretreating the sample. Impurities in the sample should have been removed due to the high calcination temperature and therefore the results should not be affected in this regard due to lack of pretreatment. However, it is possible that the catalyst contained small amounts of water after calcination and after being exposed to air at room temperature. Hydrogen spillover is sensitive to water and could affect the results. However, the amount of water in the catalyst is expected to be very low. As the support is practically non-reducible, the effect of spillover to the support can be considered small or negligible [88]. To verify that the support and instrumental factors was not interfering with the measurement, an experiment with only support material was conducted. The result showed negligible consumption of H_2 up to 950 ^{o}C.

4.4.2 Relevant Literature Results for Ni/Al_2O_3 Catalyst

In section 3.2.4 the Gibbs free energy and a reaction rate was described. Both depend on the particles themselves and their interaction with the support. The temperature ramp rate in the experiments conducted in this work was 10 ^{o}C/min. Depending on the slope of the H_2 consumption, the reduction mechanism can be determined or at least estimated. It is then necessary to determine if the temperature range in which the increase in H_2 consumption occurs can be considered constant and thereby relate to time. The aim of this would then be to determine the mechanism related to observed reduction patterns from the TPR profiles and thereby obtain information about the active species involved in the sample.

Figure 4.6 shows two reaction rate profiles common in TPR analysis of catalysts. In case A it is possible to determine a maximum reduction rate which could indicate that the reduction is being facilitated by species that are more easily reduced and is typical for auto-catalyzed reactions. While in the case of B The reduction rate is continuously decreasing which indicates that the reduction is dependent on the available surface species and as the available surface species is reduce the rate also decreases [79]. To relate this to the TPR profiles, a curve of type B would then be considered to fit with a sharp increase in H_2 consumption.

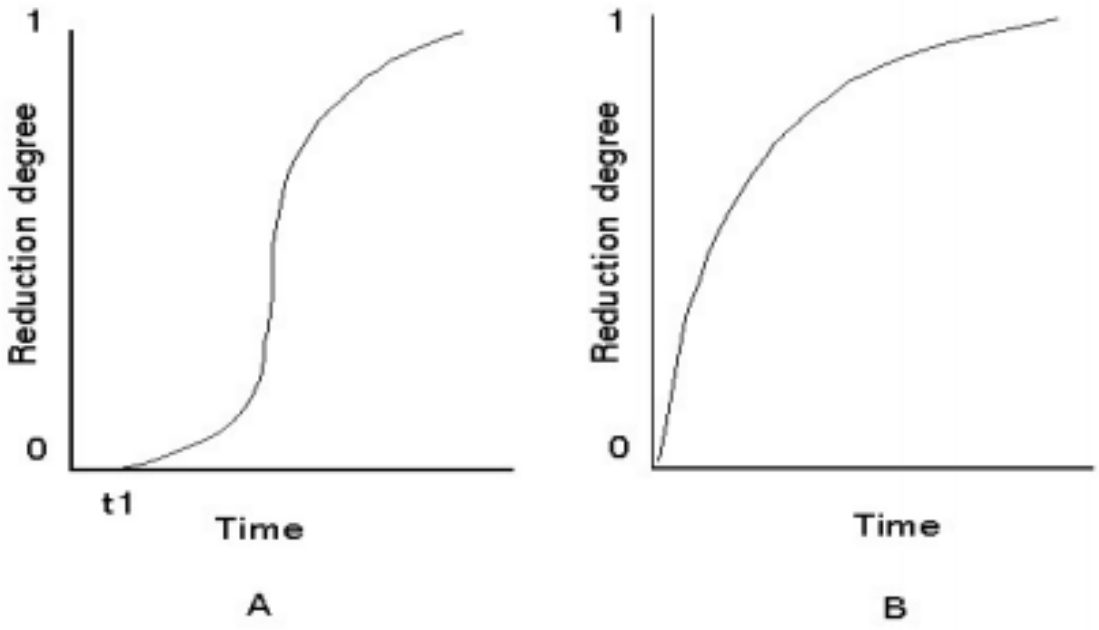

Figure 4.6: Reduction rate profiles for two reduction mechanisms *[79]*; A: Auto-catalyzed, B: Surface reduction of active species

Figure 4.7 shows the reduction temperature difference between pure NiO (a) and nickel alumina spinel (b). The Al_2O_3 support interacts with the Ni species and can thereby increases the temperature at which reduction of NiO species occur. Generally, smaller particles interact more strongly with the support and nickel alumina species is expected to be reduced above 700 ºC.

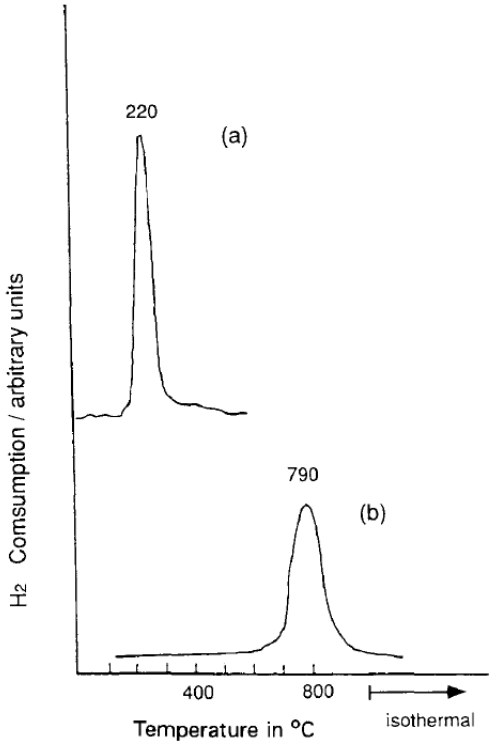

Figure 4.7: Reduction profile of (a) pure NiO and (b) $NiAl_2O_4$ *[84]*

Figure 4.8 shows the TPR profiles Ni/Al_2O_3 obtained by Li et al. [84] and the effect of Ni loading [84]. The heating rate used was 10°C/min and the sample was pretreated in flowing Ar at 400°C for 1 hour. Nickel alumina spinel species has an onset temperature during calcination of about 500 °C [89] and is therefore not observed in the TPR profiles. The peak at about 250 °C increased in intensity as the Ni loading increased. This was attributed to large particles of nickel oxide which do not form significant chemical bonds with the underlying alumina surface.

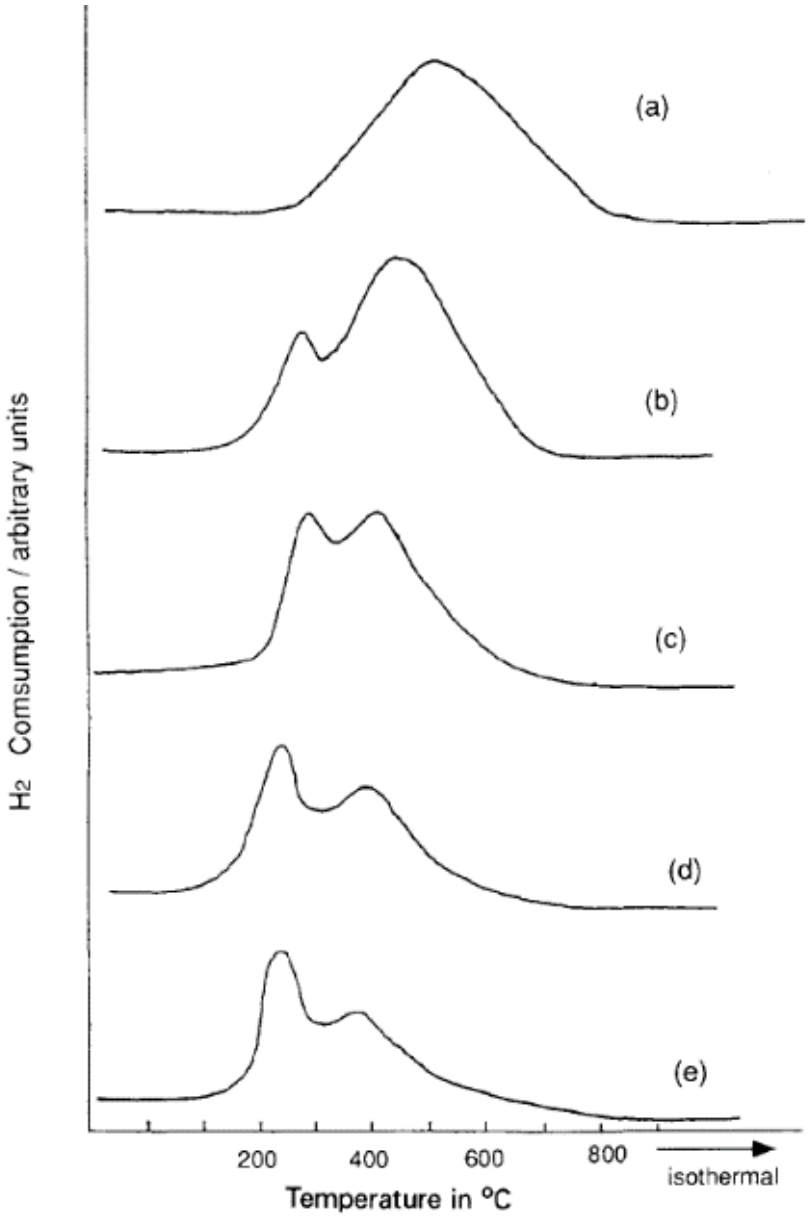

Figure 4.8: TPR profile for Ni/Al_2O_3 catalyst prepared by incipient wetness and calcined at 450 °C with Ni loading: (a) 1.8 wt%, (b) 5.3 wt%, (c) 11.3 wt%, (d) 16.4 wt%, (e) 24.8 wt%

Figure 4.8 shows a higher reduction temperature of NiO compared to the reduction temperature reported and shown in Figure 4.5. It seems that the difference in reduction temperature can be due to the preparation method of the NiO. Different types of NiO powders show large variations in behavior due to factors such as size, chemical composition, surface area, crystallinity,

temperature of calcining and content of Ni(III) [90]. Therefore, reduction of NiO species interacting with the support surface can have different reduction temperatures depending on the structure of NiO, the catalyst preparation method and to the metal-support interaction. The catalysts were calcined at 600 ºC and thus nickel alumina spinel was formed.

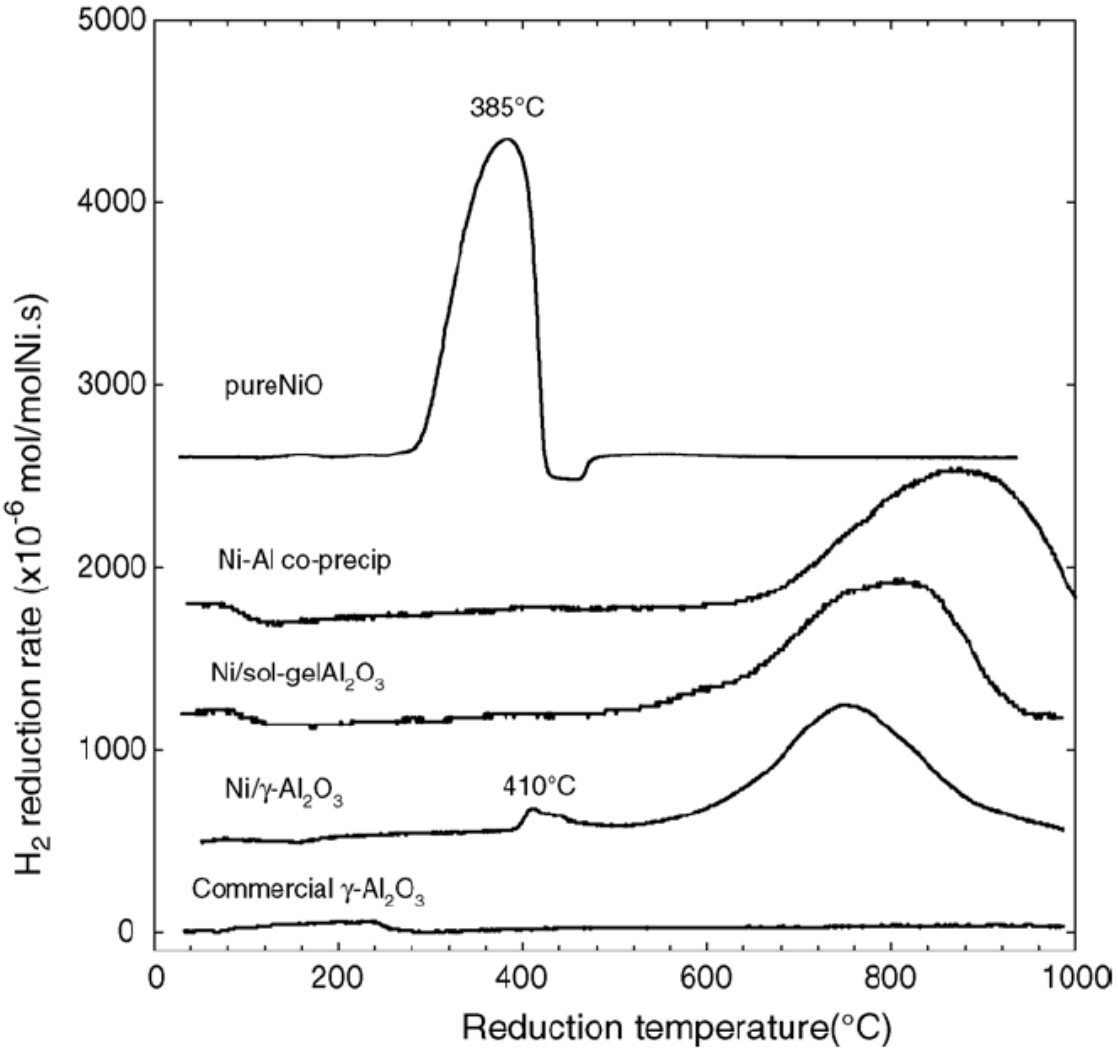

Figure 4.9: TPR profiles of Ni-Al2O3 catalysts calcined at 600 ºC, heating rate 10 ºC/min in 5% H_2 in N_2 *[91]*

The NiO used in the TPR experiment in Figure 4.7 was prepared by decomposition of $Ni(NO_3)_2x6H_2O$ at 400 ºC for 4 hours. No information was given about the preparation of the pure NiO used in the TPR experiments (Figure 4.9) and the preparation is known to affect the reduction temperature of pure NiO. However, the reduction temperature found in the two studies of pure NiO could give an indication of the reduction temperature range where free NiO species will be reduced. Free NiO are NiO particles that are not deposited at lattice sites of the support and therefore have a weak interaction with the support, resulting in a low reduction temperature [92].

4.4.3 Comparison of Ni Based Catalysts

The TPR profiles of Ni/Th and Ni/SCCa are shown in Figure 4.10. The Ni/Th catalyst was more easily to reduced. Al_2O_3 consists of tetrahedral and octahedral sites, and the nickel particles is located at both sites after preparation. If the sites are saturated, deposition as free NiO can occur on the surface of the Al_2O_3 and at defects created on the support during preparation [85]. The peak observed at 260 ^oC for Ni/Th is attributed to free NiO species. For the Ni/SCCa, the small peak at 340 ^oC is also possibly due to free NiO species. The temperature difference could be related to the particles size and/or influenced by the support.

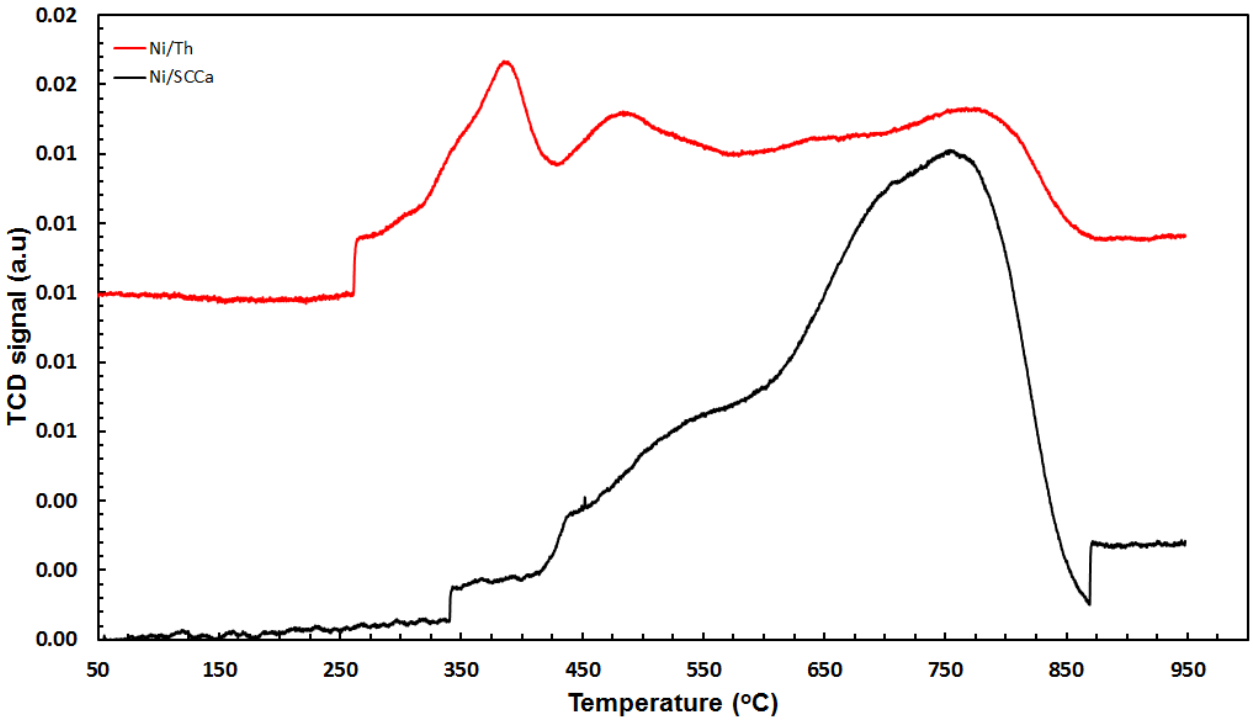

Figure 4.10: TPR profile of Ni(12 wt%)/Th and Ni(12 wt%)/SCCa catalysts calcined at 600 ^oC.

It has been shown that Ni species in interaction with tetrahedral sites of the Al_2O_3 has higher binding energy and is therefore more difficult to reduce. Molina et al. [89] provided evidence for the presence of at least two nickel species in interaction with tetrahedral and octahedral sites of the support. Thus, the peaks observed for Ni/Th at 350 ^oC and 470 ^oC could be due to different Ni species interacting with the octahedral sites. The peak at 340 ^oC for Ni/SCCa could be related to Ni species in weak interaction with octahedral sites as well. It is however clear that the NiO species of Ni/Th are more easily reduced. NiO species is expected to be reduced up to a temperature of roughly 600-700 ^oC.

During calcination, redistribution of Ni occurs between the octahedral and tetrahedral sites by diffusion. The diffusion process is related to the amount of nickel alumina spinel that is created during calcination. Two types of nickel alumina spinel can be present in the catalyst. The surface nickel alumina spinel is proposed to be more easily reduced. Bulk nickel spinel has the strongest interaction with the support and is therefore most difficult to reduce. The reduction occurring after 600 ^oC for the two catalyst is most likely due to nickel alumina spinel species. It appears that the

Ni/SCCa has a relatively higher amount of Ni interacting strongly interacting with the support. The peak at 870 ^{o}C is most likely bulk nickel alumina spinel with a strong interaction with the support.

Based on the TPR profile, the Ni/Th appears to contain larger NiO particles with a weaker interaction with the support. These NiO species are likely to be more suspect to carbon formation and sintering. In the case of Ni/SCCa, there appears to be a significant amount of Ni species that is not reduced at 600 ^{o}C. Therefore, a higher reduction temperature could have improved its catalytic performance. The large difference in reducibility can be contributed to different characteristics of the supports. Based on the results of the TPR profile, Ni/Th appear to contain larger NiO particles compared to Ni/SCCa which suggests that the crystalline size determined by dispersion experiments is highly effected by the Ni species in the catalyst.

4.4.4 TPR of Nickel Catalysts Modified by Noble Metal

Figure 4.11 shows the TPR profiles of the noble metal modified Ni/SCCa catalysts. The reducibility was improved for all modified catalyst. Pd and Pt had a peak at low temperatures which could be due reduction of PdO and PtO located at the surface of the bimetallic particles. A clear increase in H_2 consumption was not observed at low temperatures for Ru and Rh modified catalysts, which suggests that the surface concentration of RuO and RhO is low. The small peak for RhNi/SCCa at 240 ^{o}C could be due to small amounts of RhO with a weak interaction with the support [93, 94]. However, the TPR profile for Rh/Ni SCCa at low temperature could also be related to experimental concerns, such as water being present in the catalyst.

Noble metals have been known to improve the reducibility of Ni. Reduced noble metals can facilitate the reduction of NiO species through a spillover mechanism where H_2 is activated on the noble metal. The activated H_2 is dissociated to hydrogen species which can diffuse to NiO on the bimetallic particle and over the support surface [95]. This effect can be occurring on the the PtNi/SCCa and PdNi/SCCa catalyst which had a sharp peak at low temperature. In section 2.3 the bimetallic structure of nobel metals and Ni was discussed. The TPR curve could therefore indicate that a higher amount of PtO and PdO is present at the catalyst surface, whereas most of the Ru and Rh to a higher extent covered by NiO particles. The difference in H_2 consumption for Pd and Pt modified catalyst at the temperature up to 600 ^{o}C could be due to a NiO having a lower reduction temperature in the case of Pt. The difference is most likely related to the metal-support interaction which could be due to particle size and available NiO species. Pd also showed a higher H_2 consumption over 600 ^{o}C which is attributed to nickel alumina spinel.

Part of the improvement in reducibility could be related to a lesser extent of nickel alumina spinel. The noble metals are known to have a stabilizing effect on the Ni particles and thus could result in a higher amount of NiO species. A slight increase in consumption was observed for all SCCa based catalysts above 850 ^{o}C which indicates that highly stable nickel alumina spinel is present in all the catalysts. The greatest improvement in reducibility was found for PtNi/SCCa

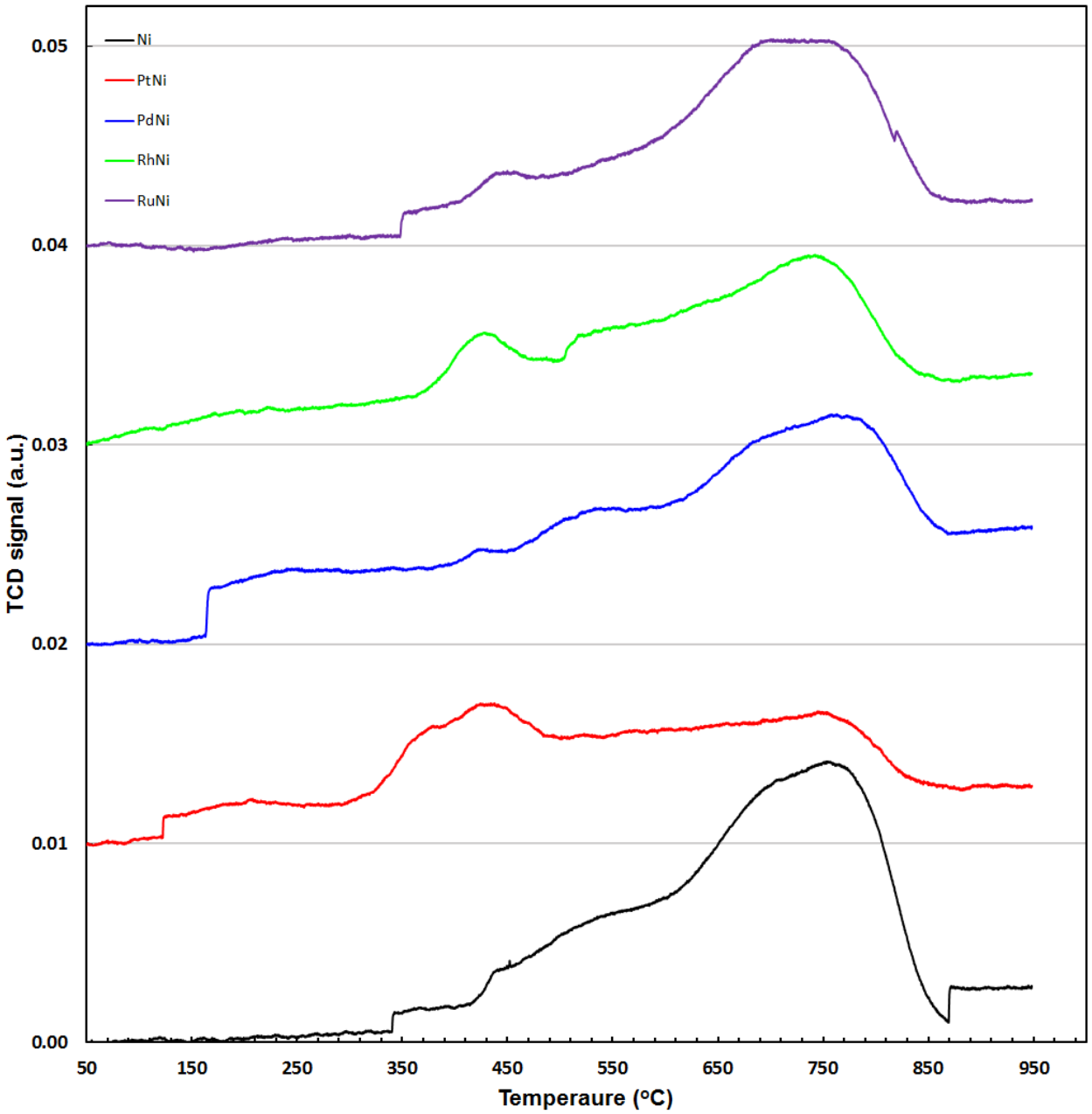

Figure 4.11: TPR profile of Ni(12 wt%)/SCCa and noble metal (0.5 wt%) modified Ni/SCCa catalysts calcined at 600 °C.

The reducibility of the modified catalysts were found to improve in the order Pt>Rh>Ru>Pd. Most of the species above 600 °C is thought to be nickel alumina spinel and thus the activity is mainly related to the NiO and noble metal oxide species on the catalysts at the activation temperature used in this work.

4.5 Catalytic activity, selectivity and deactivation

4.5.1 Experimental Concerns

The calibration of the GC gave the correct results according to the specification of the calibration gas. However, when a mixture of 50% CH4 and 50% CO2 at a total flowrate Scm3/min was flowed through the reactor, large quantities of ethylene was detected (Figure 4.12). We do not have an explanation for the appearance of ethylene but it is most probably due to errors in calibration, especially problems with the calibration gas. The amount of ethylene remained constant at room temperature. The CH4 and ethylene followed the same trend and is not expected to be produced in large quantities at dry reforming conditions. Therefore, the ethylene detected when running the catalysts have been neglected and the reported concentrations of all gases have been normalized.

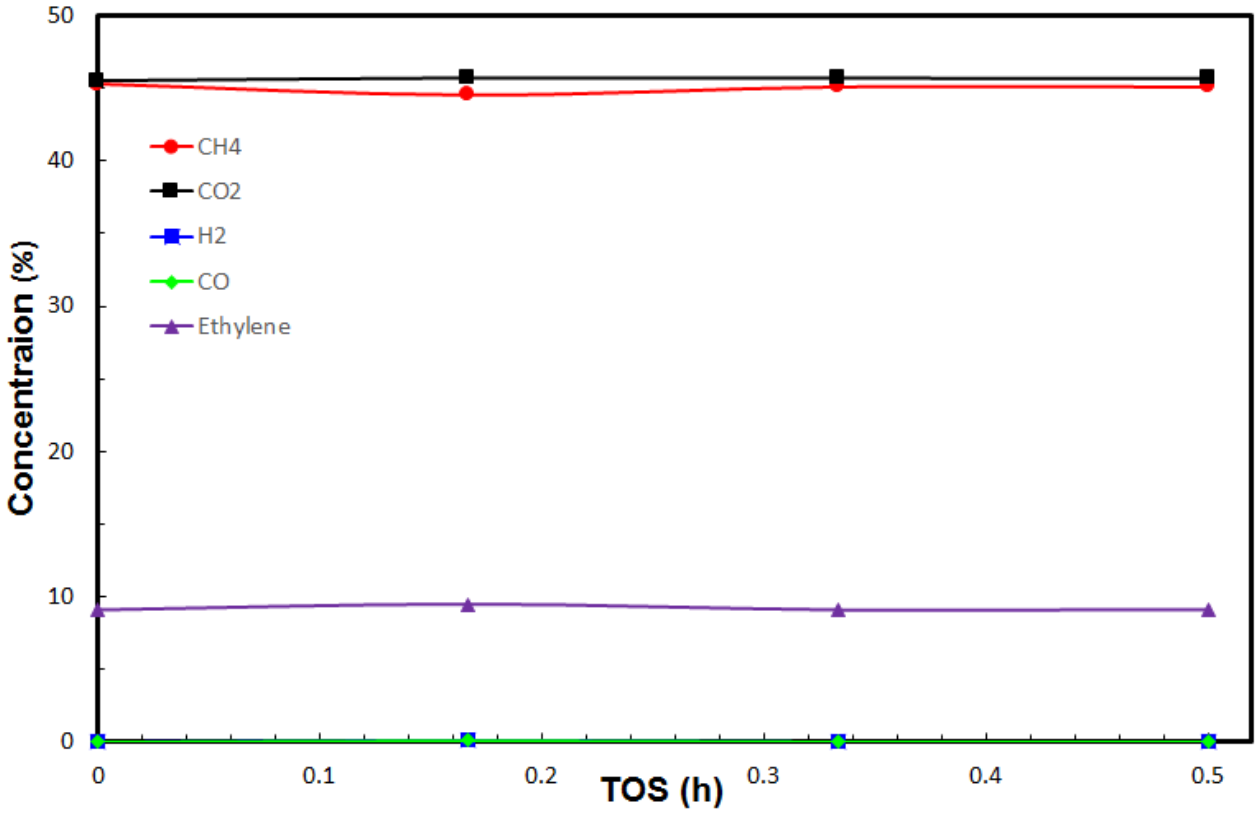

Figure 4.12: Blank experiment at room temperature with 50% CH_4 and 50% CO_2 at total flowrate 100 Scm^3/min.

The stainless steel reactor contained a smaller steel tube with internal diameter of 9mm. Carbon deposits was observed along the tube wall of the reactor but most of the deposited carbon was inside the smaller tube. The small tube was plugged with quartz wool and on top was the catalyst diluted with γ-Al_2O_3. After each, experiment the carbon deposits throughout the reactor were checked and almost no black carbon was found in the catalyst bed. The quartz plug did not contain any black carbon, except for part that was in contact with the tube wall. Therefore, the cause of the carbon deposits appears to be related to the tube wall. At blank experiments at 700 ^oC and a flowrate of 100 Scm^3/min with 50% CH_4 and 50% CO_2, the conversions was less

than 0.5 % (0.2-0.5%) and the result are shown in Figure 4.13. Therefore, the effect of the reactor tube could be neglected.

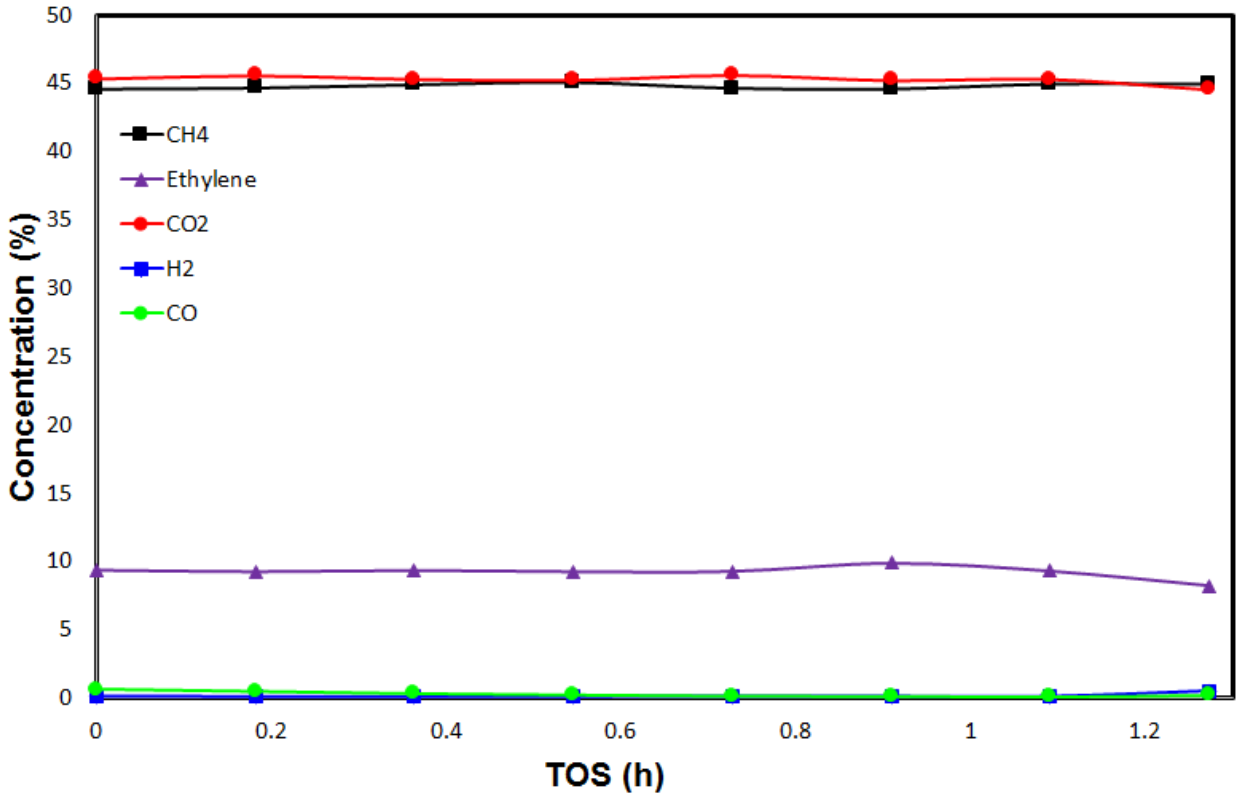

Figure 4.13: Blank experiment at 700 ^{o}C with 50% CH_4 and 50% CO_2 at total flowrate 100 Scm^3/min.

The amount of carbon that was deposited inside the small tube was not directly measured and most of it was very difficult to remove. Figure 4.15 shows the catalyst diluted in γ-Al_2O_3 to the left and to the right a small amount of the deposited carbon with the quartz plugs. The total volume of carbon deposited in the small tube was much larger than the volume of the catalyst/Al_2O_3 mixture. As the blank experiments at 700 ^{o}C showed almost no conversions at the flowrate used during the experiment the effects on the result is expected to be minimal. The carbon deposits suggest that the reactor design is not optimal for DRM as there are reactions occurring after catalyst bed. It appears that the reaction is. At 650 ^{o}C there was small amounts of carbon deposited in the small tube and at 600 ^{o}C the carbon deposits were negligible. Thus the deposits in the small tube is expected to be due to low conversions occurring in the small tube and leading to a slow buildup of carbon. During tests at 800 ^{o}C the small stainless steel tube was blocked after about 15 hours. Thus the experiments were conducted at 700 ^{o}C to try to minimize the effect of the reactor.

Figure 4.14: Left: Catalyst diluted in y-Al2O3; Right: fraction of deposited carbon in the small stainless steel tube and quartz wool plugs

4.5.2 Relevant literature results for Ni/Al_2O_3 catalysts at high GHSV

The gas hourly space velocity (GHSV) used in the experiments was 120 000 $\mathrm{Scm}^3\ \mathrm{g}_{\mathrm{cat}}^{-1}\ \mathrm{h}^{-1}$ which is too high to evaluate the results in accordance with equilibrium conversions. Figure 4.15 shows the influence of GHSV on the conversions found by J. Newnham et al. [92]. The catalyst was a 10 wt% Ni on mesoporous alumina, prepared by a modified co-precipitation method. The conversion was found to reduce significantly with increasing GHSV and the deactivation rate is also higher, especially at 120 000 GHSV. In addition, the H_2:CO molar ratio was also found to be dependent on the GHSV.

A higher GHSV results in a lower contact time which means that the CO_2 and CH_4 molecules have less time to interact with the active sites. The limited residence time can thus result in lower conversion of CH_4 and CO_2 compared to the equilibrium conversion. Another factor that has to be taken into account is the dispersion of the active sites. If the active particles are small enough and well dispersed throughout the pores, the loss in conversion will be low compared to larger particles. The pores could also come into play at high GHSV as the mass transfer inside the pores is likely to depend on the pore size. There is not enough information obtained about the pore distribution of the catalyst in the textural properties and therefore the effect of the pores is considered to be smaller compared to the impact of the nickel particle size.

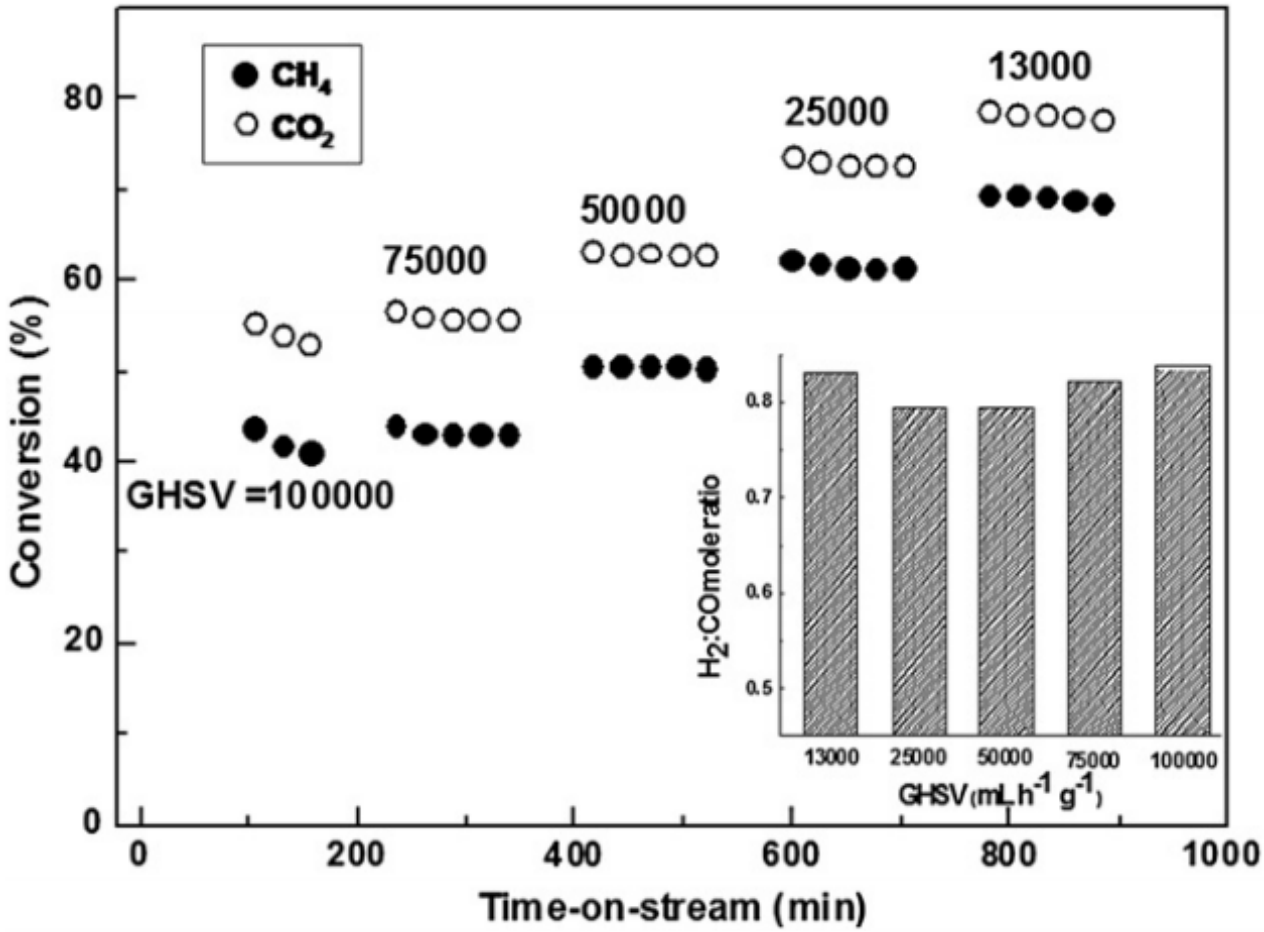

Figure 4.15: Influence of GHSV of feed gas mixture on the conversions of CH_4 and CO_2, bottom right: H_2:CO product mole ratio, over Ni (10 wt%) - mesoporous alumina prepared by modified co-precipitation method at 700 ^oC *[92]*.

Figure 4.16 shows the relation between particle size and particle distribution found by Rahemi et al. [96]. They found that the catalyst with the highest amount of small particles almost showed constant activity at GHSV of 24000 to 60000 $Scm^3/g^{-1}h^{-1}$. The decline in conversion rate was enhanced as the particle size increased. In addition, the conversion of two catalysts with a high decline rate converged with increasing GHSV. Thus it appears to be difficult to determine the catalytic performance at or close to equilibrium conditions based on high GHSV data.

The effect of the GHSV has not been investigated in this thesis. Thus a decreasing trend as depicted in figure 4.15 is therefore assumed in the analysis of the catalytic performance, as well as that the activity order of the catalyst would not change at lower GHSV.

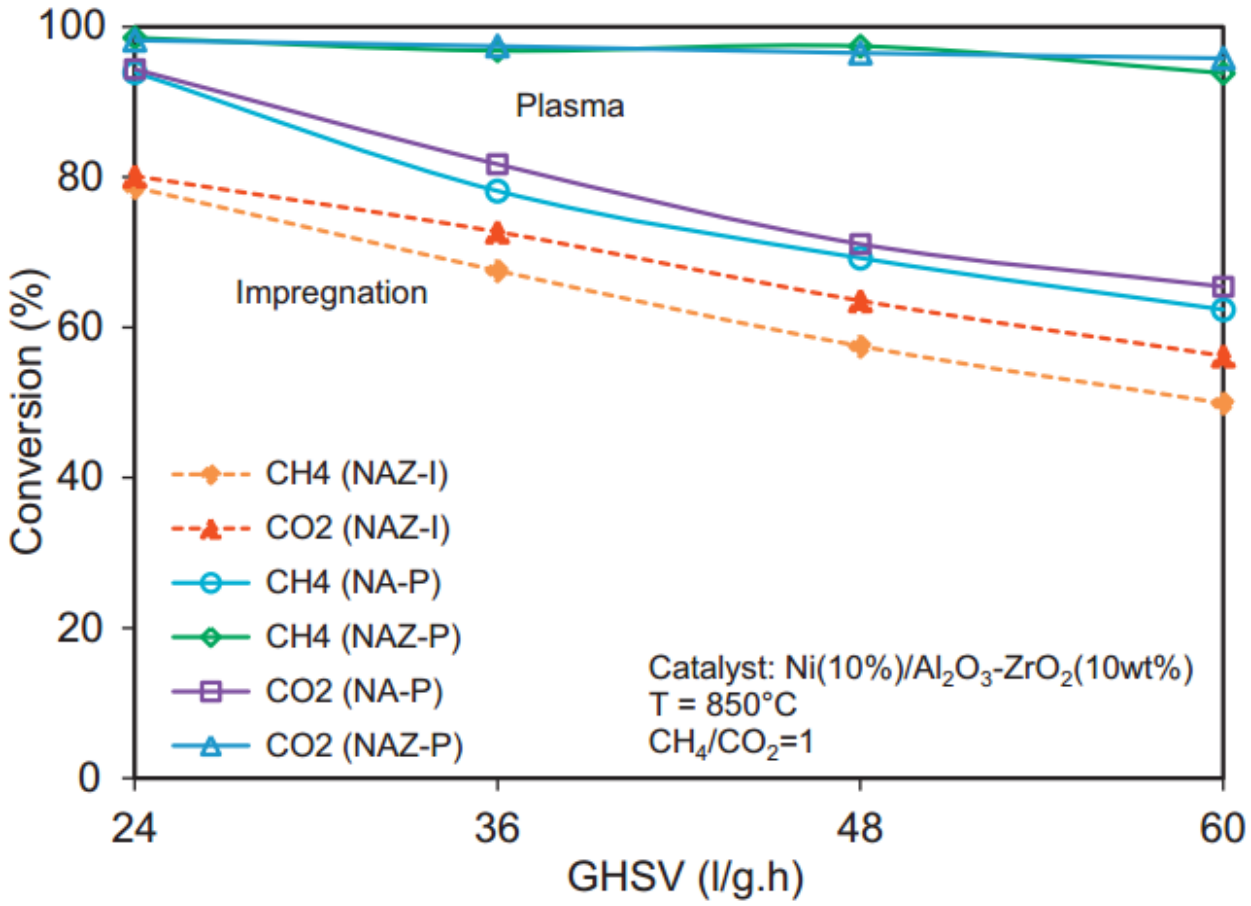

Figure 4.16: The effect of GHSV on conversion feed conversion: Ni-Al_2O_3-ZrO_3 prepared by impregnation (NAZ-I) with average particle size 57.7 nm, Ni-Al_2O_3 plasma treated (NA-P) with average particle size 35.8 nm and Ni-Al_2O_3-ZrO_3 plasma treated (NAZ-P) with average particle size 35.3 nm *[96]*.

4.5.3 **Catalyst performance**

The conversion of CH_4 and CO_2 for the monometallics Ni catalysts are presented in Figure 4.17. The conversions were higher for Ni/Th throughout TOS (15 h) and was attributed to the higher amount of active Ni particles after reduction. Both catalysts showed initial higher conversion of CO_2 which converged towards the CH_4 conversion with TOS. The catalyst precursor has been shown to affect the CO_2 conversion by altering the surface basicity [97]. They found that Ni nitrate precursor had the highest surface basicity and resulted in increased CO_2 conversion and improved regasification rate of deposited carbon. The proposed mechanism is that CO_2 is activated on the support's basic sites and diffuse over the support surface to active particles. The observed high initial conversion of CO_2 for both catalysts can be related to the surface basic sites and the regasification rate which is likely to be higher initially due to a higher carbon deposition rate.

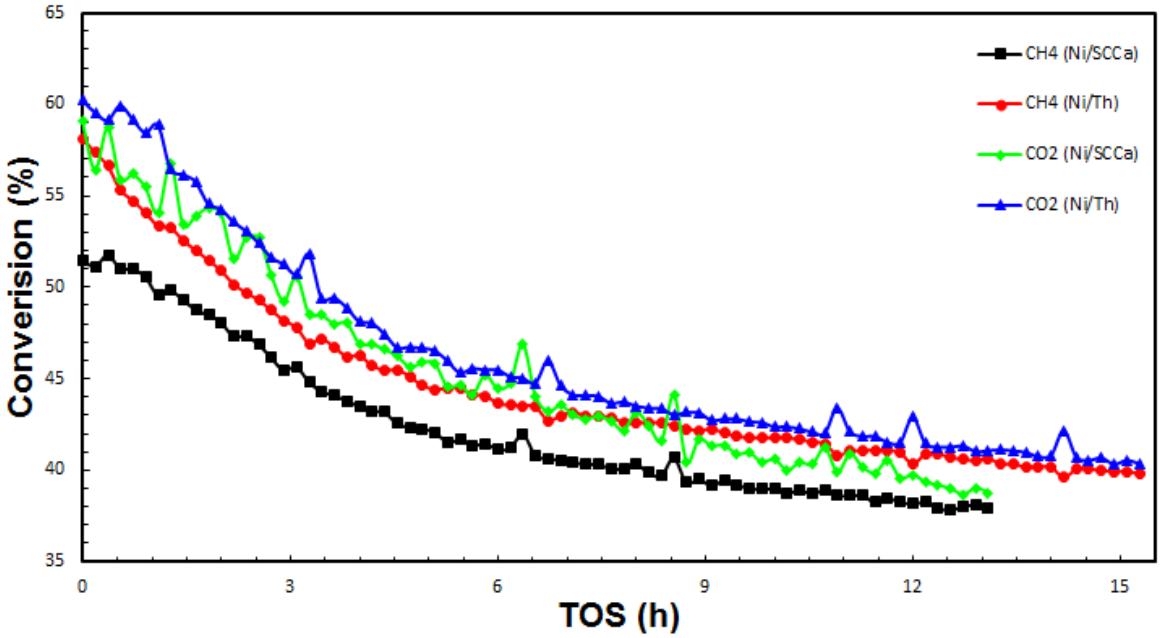

Figure 4.17: Conversions of CH_4 for monometallic Ni/γ-Al_2O_3 catalysts

Fluctuations were observed in CO_2 and CH_4 conversions throughout TOS and could be related to instability in the carbon deposition/utilization cycles [63]. Ni/Th showed a higher initial deactivation rate which is attributed to the presence of larger particles being more rapidly deactivated through carbon deposition. After 13 hours, both catalysts showed a linear deactivation rate which is likely due to carbon deposition and sintering of Ni particles.

The H_2 and CO selectivity and the H2/CO ratios of the monometallic Ni catalysts are shown in Figure 4.18.

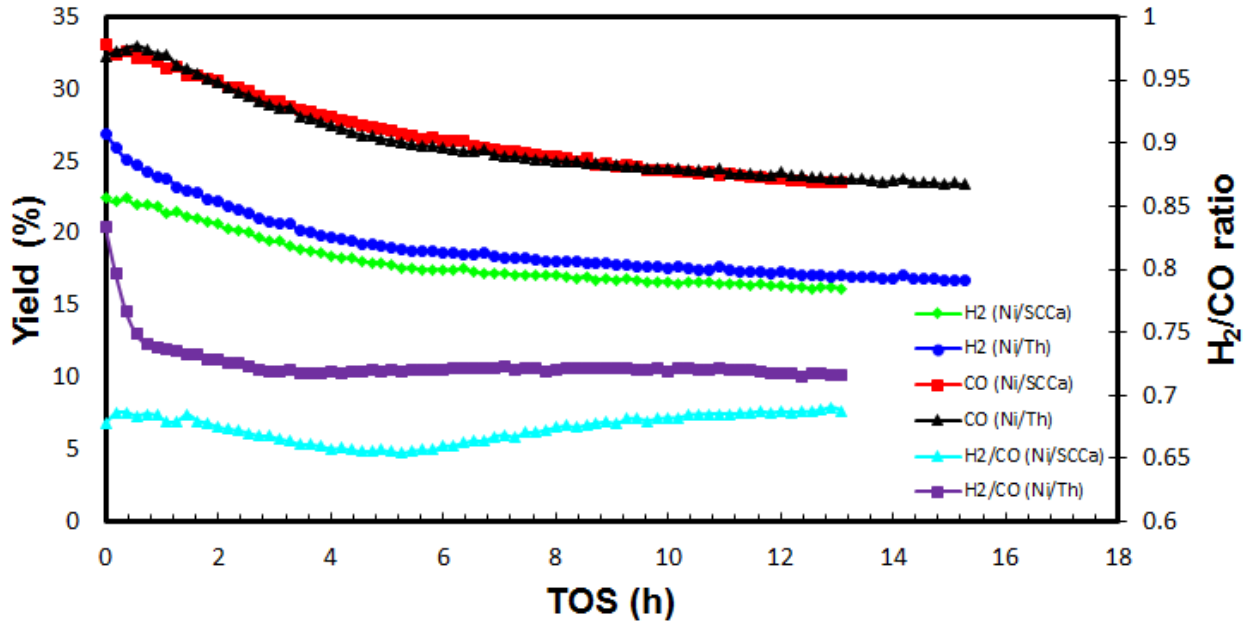

Figure 4.18: Product selectivity and H_2/CO ratio of monometallic Ni catalysts

The CO yield for both catalysts were similar but Ni/Th had a higher H_2 yield. The difference in H_2 yield is attributed to a higher initial conversion of CH_4 for the Ni/Th catalyst. The incease in H_2/CO ratio for Ni/SCCa is due to different decline rate for H_2 and CO yield. The constant decline for the CO yield might be related to the support. The activation of CO_2 appears to be maintained at a higher level and could be due to higher support stability and the interfacial zone between the Ni particle and the support. The initial rapid decrease in H_2/CO ratio for Ni/Th is attributed to inactive carbon species.

The CH_4 conversion of the SCCa supported catalysts is shown in Figure 4.19. The noble metal modified catalysts showed improved activity, except for the Pd modified catalyst which also showed the highest deactivation rate. Pd has been found to both have a positive and negative effect by other studies (Table 2.2). The loading amount has been shown to be important in regards to Pd-Ni catalysts. At low Pd/Ni ratios the Pd was found to improve the catalytic performance where an optimum was found at 0.07 [52]. A different study used a Pd/Ni ratio of 0.3 which was found to reduce the activity and stability compared to the monometallic Ni catalyst [58]. The theoretical ratio used in this work was 0.04 but the active particles that were reduced at 600 ^oC might have a higher ratio due to nickel alumina spinel. The TPR indicated that the Pd-Ni catalyst contained more reducible Pd species than Pt, which might suggest that a higher amount of Pd is present at the surface of the bimetallic particles. Thus, the reduction in activity and stability could be due to the actual Pd/Ni ratio of the active species in the catalyst. The results obtained for the Pd suggest that the nickel alumina spinel must be controlled to achieve improvements in reducible species and possibly a more optimal Pd/Ni ratio in the active particles.

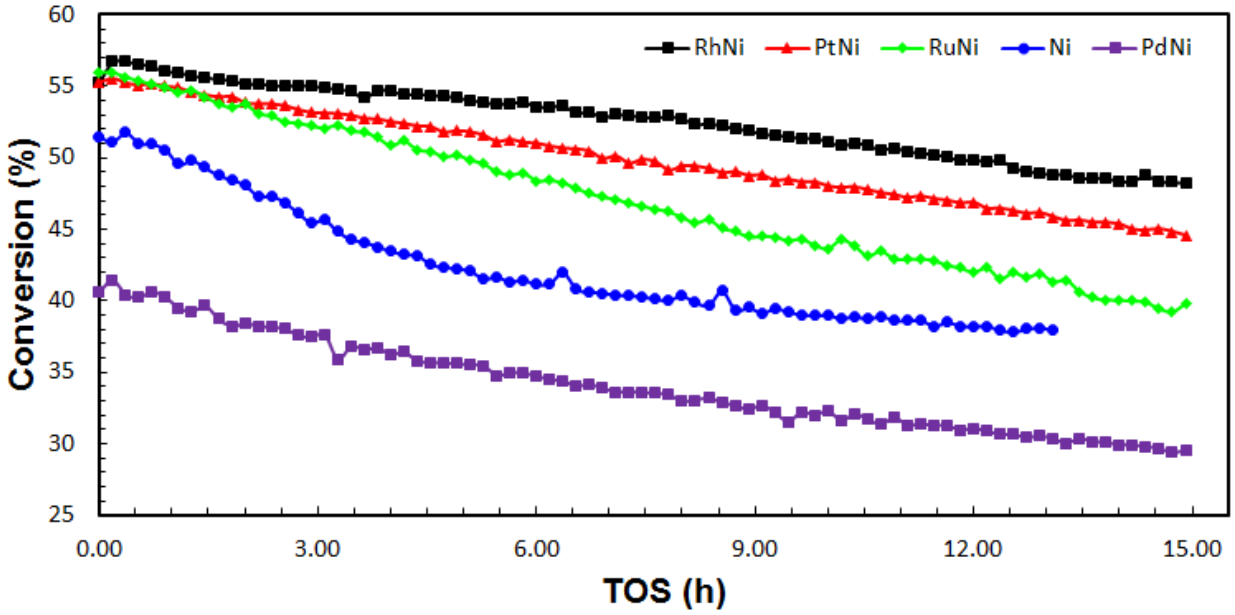

Figure 4.19: CH_4 conversions for noble metal (0.5 wt%) – Ni (12 WT%) catalysts at 700 ^oC and GHSV 120,000 $Scm^3 g^{-1} h^{-1}$.

Although the Ru-Ni catalyst showed higher initial conversion than the Ni catalysts, the deactivation rate was higher. This could be due to the presence of larger particles. Rh-Ni showed the highest activity, followed by Pt-Ni. The CH_4 conversion decline rate was relatively

constant for the bimetallic catalysts. It could be related to more stable particles, a higher resistance to carbon deposition and that the deposited carbon had a higher activity.

Figure 4.21 shows the conversion of CO2 for the SCCa based catalysts. The Ru-Ni catalyst showed better conversion for CO_2 which could be due to favoring the conversion of CO_2. On the other hand, the Rh-Ni catalyst suggest the opposite, and Rh has been found to favor the conversion of CH_4 by other researchers (section 2.2 and 2.3). It can be seen that there possibly is a rapid deactivation of for Rh-Ni in the beginning for the CO_2 conversion. This could be due to the deactivation of Ni active sites due to carbon deposits. Thus the synergetic effect of Rh and Ni appears to be maintained where Rh is favoring the conversion of CO_2 and Ni accounting for most of the conversion of CO_2.

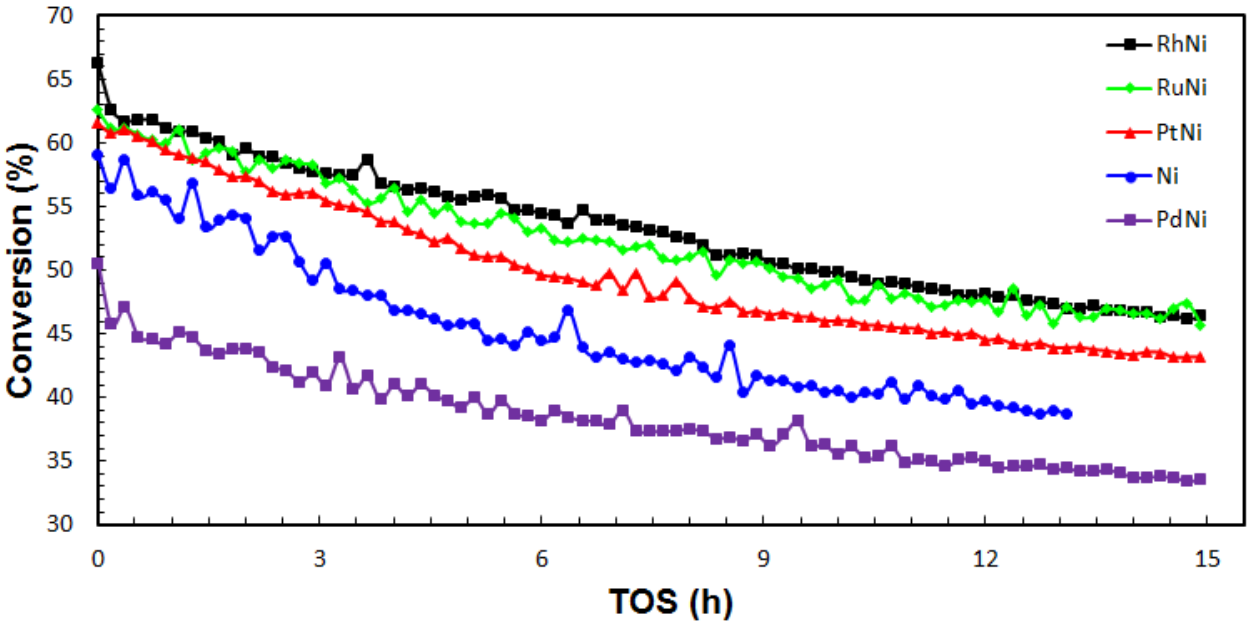

Figure 4.20: CO_2 conversions for all the catalysts at 700 ^oC and GHSV 120,000 $Scm^3\ g^{-1}\ h^{-1}$.

The support might also be contributing to the CO_2 conversion for the noble metal modified catalysts as the difference in CO_2 conversion is smaller compared to the conversion of CH_4. The selectivity of H_2 is shown in Figure 4.22 and the CO selectivity in Figure 4.23. At 700 ^oC the yield of H2 is supposed to be higher than the yield of CO based equilibrium calculations. However, the catalyst is known to affect the reaction rates which could alter the achieved H_2 and CO yield [14]. In addition to the effect of the catalysts, the high GHSV used in these experiments could result in a higher yield of CO_2. CO_2 can be activated on the support's basic sites as well as being converted at the active sites, which could result in deviations from the yield obtained at equilibrium conversion.

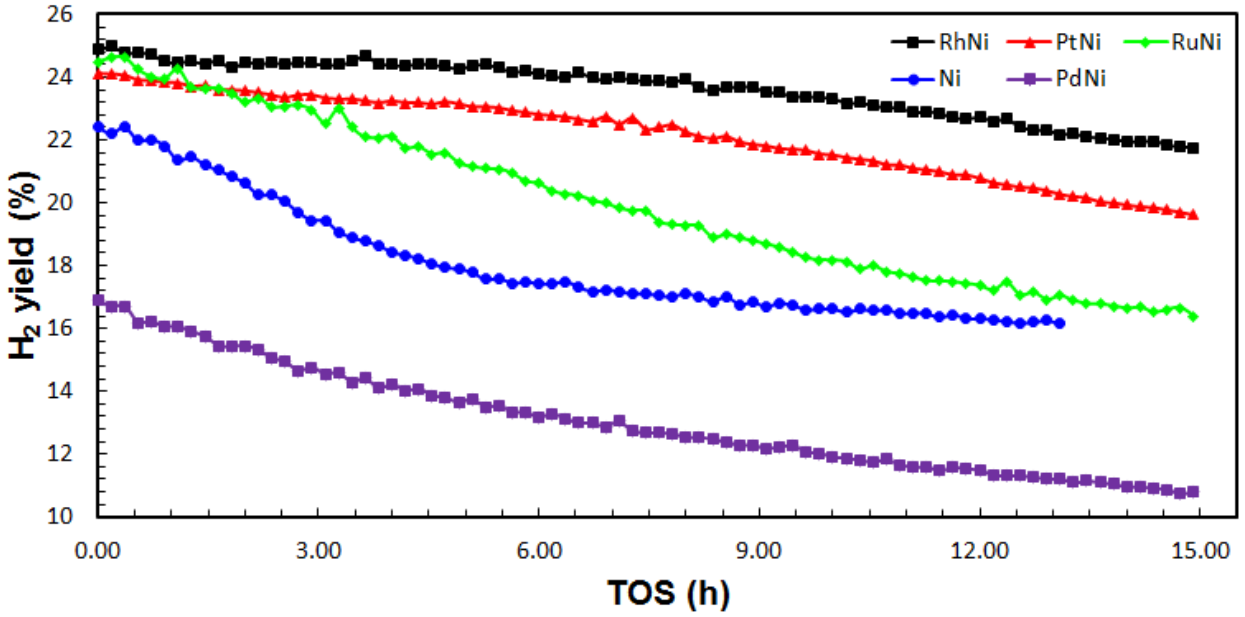

Figure 4.21: Selectivity of H_2 for all catalysts at 700 ^oC and GHSV 120,000 $Scm^3\ g^{-1}\ h^{-1}$.

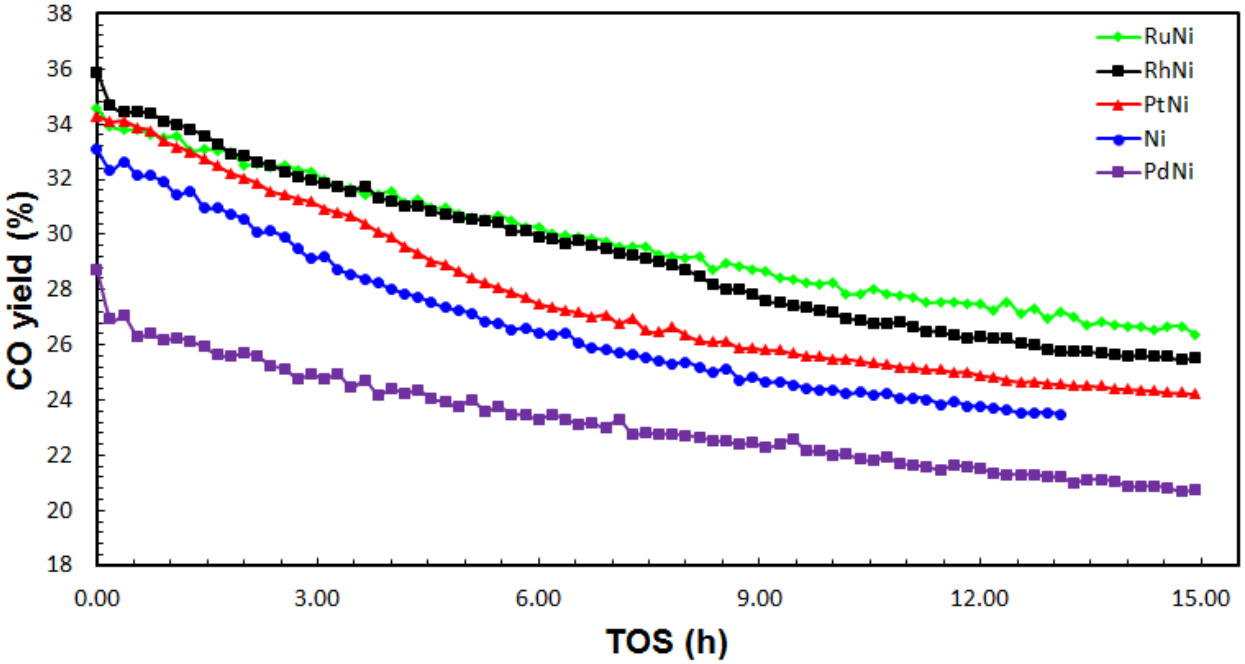

Figure 4.22: Selectivity of CO for all catalysts at 700 ^oC and GHSV 120,000 $Scm^3\ g^{-1}\ h^{-1}$.

The H_2/CO ratio is shown in Figure 2.24 and the RWGS reaction (Eq. 1.8) is also known to affect the ratio. The catalyst investigated was found to have different H_2/CO ratio which varied with TOS. It appears that the that the CH_4 and CO_2 conversions for the catalysts did not follow the same deactivating trend and rate. For example, the Rh-Ni catalyst had low deactivation of CH_4 and stable H_2 yield in the beginning, while the CO_2 and CO yield was decreasing. Thus in the beginning the H_2/CO ratio is increasing. After about 11,5 hours TOS, the conversion of CH_4

and H_2 yield is decreasing while the CO_2 conversion and CO yield is stabilizing, which leads to the H_2/CO ratio decreasing.

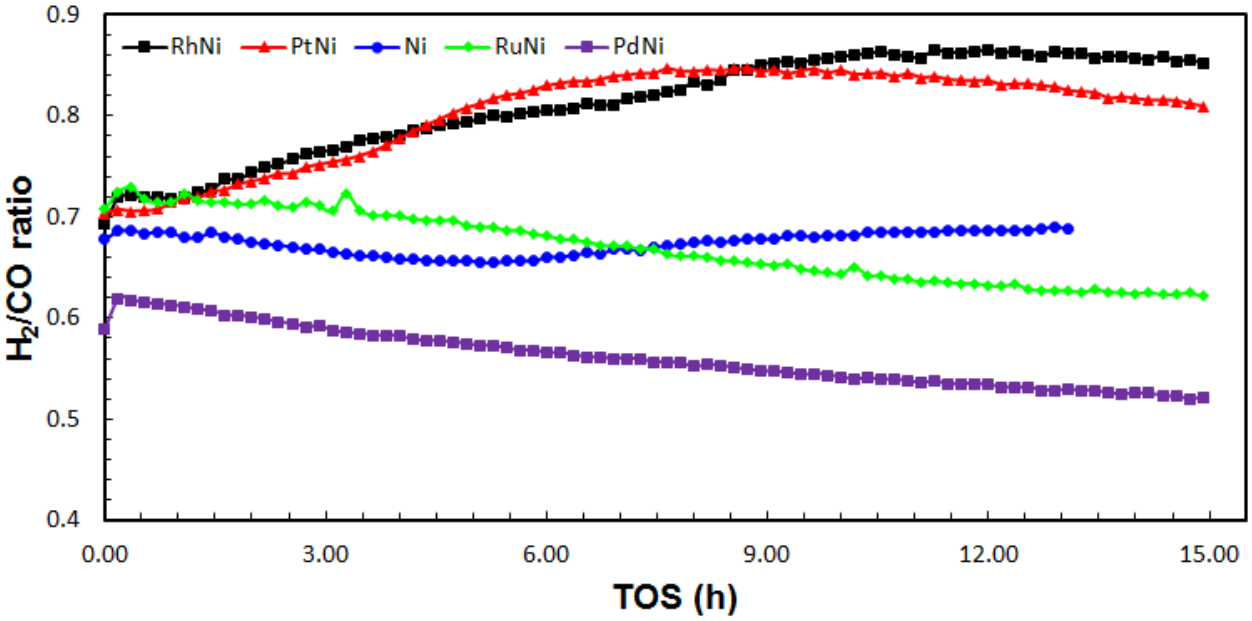

Figure 4.23: H2/CO ratio for all catalysts at 700 °C and GHSV 120,000 $Scm^3\ g^{-1}\ h^{-1}$.

The Pd-Ni and Ru-Ni catalysts have a constant decline in H_2/CO ratio. This is due to a higher deactivation rate for CH_4 conversion and H_2 yield compared to CO_2 conversion and CO yield. The deactivation of the catalyst appears to not only depend on the active metal particles, but possibly also on the support for all the catalyst.

4.5.4 Effect of temperature on DRM for RhNi/SCCa catalyst

To investigate the effect of temperature, the Rh(0.5 wt%)Ni(12 wt%)/SCCa catalyst was tested at 700 °C, 650 °C and 600 °C at a GHSV of 120,000 Scm^3/min. The conversion and stability characteristics of the catalyst is presented in Figure 4.25, and the different decline rates for CH_4 and CO_2 is well illustrated. In addition to the CO_2 conversion corresponding to the RWGS reaction, the improved conversion is proposed to be related to the basic sites of the support. The amount of basic sites on the support was found to increase with activation temperature [98]. Oxygen vacancies in the alumina structure corresponds to Lewis basic sites. Parts of the CO_2 conversion might be related to oxygenation of the oxygen vacancies in the support structure. The activation of CO_2 is therefore proposed to both supply oxygen to carbon species on the active metal and oxygen vacancies. The decline in CO_2 conversion therefore appears to be related to both the catalyst and the support.

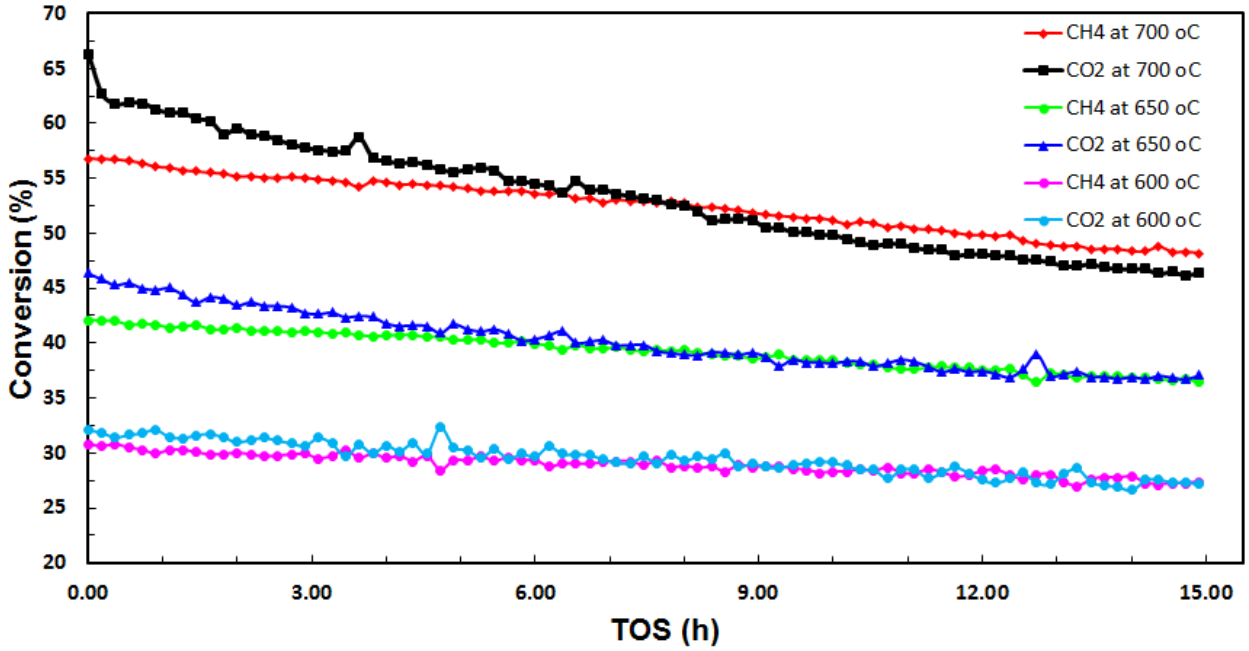

Figure 4.24: Conversion of CO2 and CH4 dependence on temperature for RhNi/SCCa at 600, 650 and 700 ^{o}C and GHSV 120,000 Scm^{3} g^{-1} h^{-1}.

The conversion is dramatically reduced as expected when the temperature is decreased. The deactivation rate for CH_4 conversion is declining constantly at all the temperatures. The CH_4 and CO_2 deactivation rate is also lower at 650 and 600 ^{o}C. Numerical values for the conversions and relative decline rate are shown in Table 4.5.

Table 4.3: Catalyst activity and stability for Rh(0.5 wt%)Ni(12 wt%)/SCCa with GHSV 120,000 Scm^{3} g^{-1} h^{-1} at different temperatures.

0.5Rh12Ni/SCCa	Initial conversion (%)	Conversion at end (%)	Decrease relative to initial conversion (%)
CH_4 at 700 ^{o}C	56.8	48.2	15.2
CO_2 at 700 ^{o}C	62.2	46.4	25.4
CH_4 at 650 ^{o}C	42.1	36.4	13.4
CO_2 at 650 ^{o}C	46.3	36.7	20.7
CH_4 at 600 ^{o}C	30.8	26.9	12.7
CO_2 at 600 ^{o}C	32.1	27.15	4.95

The carbon deposition rate has been found to increase as the temperature decreases based on a thermodynamic equilibrium analysis [81]. The improved CO_2 disassociation due to the precursor used, the support and the improved resistance to carbon deposition by Rh can partly

be the reason. In addition, the high GHSV reduces the activity at lower temperatures by a greater amount than at equilibrium calculations, resulting in a lower carbon deposition rate.

The H_2/CO ratio is shown in Figure 4.26. The H2/CO ratio is also decreasing at lower temperature. Equilibrium calculations by Nikoo and Amin [81] shows that the H_2/CO ratio is reduced at lower temperature. The catalyst is known to affect the ratio. A study conducted on Pt(Na(0.3 wt%)-Al_2O_3 catalyst by E. L. Jablonski et al. showed the same trend with decreasing temperature [99]. In this work both the catalyst and the GHSV used is proposed to have affected the H_2/CO ratio.

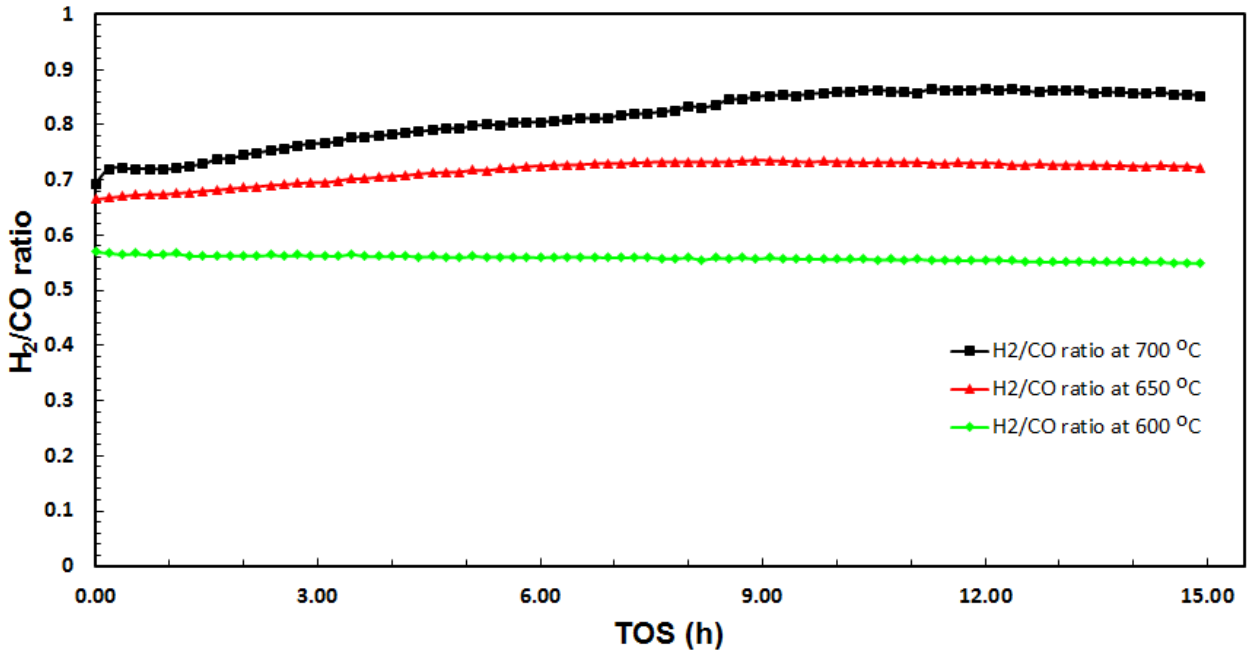

Figure 4.25: Catalyst selectivity for RhNi/SCCa at 600, 650 and 700 °C at GHSV 120,000 $Scm^3\ g^{-1}\ h^{-1}$.

The decline in CH_4 and CO_2 conversion to temperature relative to equilibrium calculations is also decreasing by a faster rate, which suggests that at higher GHSV the reduction in conversions is further enhanced.

5 Conclusion and recommendations for Future Work

The aim of this thesis was to compare alumina supported nickel based catalysts with modified catalysts with small amounts of noble metals and suggest further focus in catalyst development.

5.1 Conclusion

Dry reforming of methane to produce CO-rich synthesis gas with a more suitable H_2/CO ratio was studied. The work focused on catalytic development to improve catalyst activity and stability through modifying Ni(12 wt%)/γ-Al_2O_3 with low amounts of noble metals (0.5 wt%). A different support was synthesized with 12% nickel loading to compare the effect of the support. The catalysts were prepared by the incipient wetness method and underwent the same preparation procedure.

The textural measurements showed a decrease in surface area after impregnation and the noble metal modified catalysts did not improve the surface area. Based on the XRD and TPR experiments conducted, a high amount of nickel alumina spinel was present in all the catalyst. The amount was different for the two monometallic Ni catalyst which suggests that the amount of nickel alumina spinel produced during calcination is partly related to properties of the support. The noble metal modified nickels catalyst was found to inhibit the extent of nickel alumina spinel development to a varying degree. Improvement in reducibility was also found for the modified with catalysts.

Activity and stability was investigated at 700 ^oC and GHSV of 120,000 $Scm^3/min\ g^{-1}\ h^{-1}$. The monometallic catalyst with the lowest amount of nickel alumina spinel showed the highest conversion of the feed gases, but the lowest stability. The nickel alumina spinel development improves the dispersion of the NiO phases and thus result in smaller particles with a higher stability. The difference in activity was attributed to a higher amount of active sites at the reduction temperature of 600 ^oC. Rh showed the highest activity and stability of the modified catalysts, followed by Pt and Ru. On the other hand, the addition of Pd resulted in a decrease in activity and stability for the modified nickel alumina catalyst.

The effect of temperature on catalytic performance was conducted on the Rh modified catalyst at a GHSV of 120,000 $Scm^3/min\ g^{-1}\ h^{-1}$. The conversions were found to decreased with temperature at a higher rate compared to estimates based on equilibrium calculations. In addition, the H_2/CO ratio decreased at lower temperature, contradicting equilibrium calculations. The deactivation rate was also found to decrease with temperature. This is attributed to improvements in carbon inhibition caused by Rh and the lowered activity at high GHSV.

5.2 Recommendations for Future Work

Nickel catalyst modified by noble metals has been shown to improve the catalyst. Based on research discussed in section 2.3, the noble metal to nickel ratio have been shown to be of importance. The optimal ratio depends on factors such as the noble metal, the support used and bimetallic particle structure. The incipient wetness method resulted in a varying amount of nickel alumina spinel for the noble metal modified catalysts in this work. Thus the nickel content remaining in the bimetallic particles could be difficult to optimize through this preparation method without modifications. The bimetallic particle structure itself would also be challenging to control.

Therefore, preparation methods that offer better control on the particles and structure of the catalyst could be used to give more accurate information about the bimetallic synergy and improve the catalyst. Rhodium followed by platinum was found to show the greatest potential in this work, but the other noble metals have been reported to be promising as well and should be further investigated.

References

[1] ExxonMobil, "ExxonMobil The Outlook for Energy: A View to 2040," 2016.

[2] Intergovernmental Panel on Climate Change, "Fifth Assessment Report, Mitigation of Climate Change," 2014.

[3] European Commission Climate, "http://ec.europa.eu/clima/policies/strategies/2030/index_en.htm".

[4] Eva k. Halland, Wenche T. Johansen., Fridtjof Riis, Rune Goa, Arne Bjørøen, Janne N'Jai (Norwegian petroleum Directorate), "CO2 Storage Atlas Norwegian North Sea". *http://www.npd.no/Global/Norsk/3-Publikasjoner/Rapporter/PDF/CO2-ATLAS-lav.pdf.*

[5] Peter Styring (The University of Sheffield), D.J.E., "Carbon Capture and Utilisation in the green economy," 2011.

[6] M. Limbach and S.A. Schunk, "Acrylates from alkenes and CO2, the stuff that dreams are made of," *Symposium CO2 als Wertstoff,* 2012.

[7] Rostrup-Nielsen, J.R., J. Sehested and J.K. Nørskov, "Hydrogen and synthesis gas by steam-and CO2reforming," *Advances in Catalysis 47,* pp. 65-139, 2002.

[8] S. Ghoneim, R. El-Salamony, and S. El-Temtamy, "Review on Innovative Catalytic Reforming of Natural Gas to Syngas.," *World Journal of Engineering and Technology, 4,* pp. 116-139, 2016.

[9] L.S. Neiva and L. Gama , "A Study on the Characteristics of the Reforming of Methane: A Review.," *Brazilian Journal of Petroleum and Gas, 4,* pp. 119-127, 2010.

[10] C. Palm, P. Cremer, R. Peters and D. Stolten, "Small-Scale Testing of a Precious Metal Catalyst in the Au-to-Thermal Reforming of Various Hydrocarbon Feeds," *Journal of Power Sources, 106,* pp. 231-237, 2002.

[11] X. Song and Z. Guo, "Technologies for Direct Production of Flexible H2/CO Synthesis Gas.," *Energy Conversion and Management, 47,* pp. 560-569, 2006.

[12] A.M. Gadalla and B. Bower, "The Role of Catalyst Support on the Activity of Nickel for Reforming Methane with CO2," *Chemical Engineering Science, 43,* pp. 3049-3062, 1988.

[13] Ahmed Sadeq. Al-Fatesh, Ahmed Aidid. Ibrahim, Sajjad Haider and Anis Hamza. Fakeeha, "Sustainable Production of Synthesis Gases via State of the Art Metal SupportedCatalytic Systems: An Overview, Journal of the Chinese Chemical Society, Volume 60, Issue 11, pages 1297–1308, November 2013".

[14] M. Khoshtinat Nikoo and N.A.S. Amin, "Thermodynamic analysis of carbon dioxide reforming of methane in view of solid carbon formation," *Fuel Processing Technology Volume 92, Issue 3,* p. 678–691, 2011.

[15] Z. Hou, P. Chen, H. Fang, X. Zheng and T. Yashima , "Production of Synthesis Gas via Methane Reforming with CO2 on Noble Metals and Small Amount of Noble-(Rh) Promoted Ni Catalysts," *International Journal of Hydrogen Energy, 31,* pp. 555-561, 2006.

[16] G. S. Gallego, C. Batiot-Dupeyrat, J. Barrault, E. Florez, F. Mondragon, "Dry reforming of methane over LaNi1-yByO3-d (B = Mg, Co) perovskites used as catalyst precursor," *Appl. Catal. A. 334 (1),* p. 251−258, 2008.

[17] D. Chen et al., "Deactivation during carbon dioxide reforming of methane over Ni catalyst: microkinetic analysis," *Chemical Engineering Science, 56(4),* pp. 1371-1379, 2001.

[18] F.F. de Sousa et al., "Nanostructured Ni-containing spinel oxides for the dry reforming of methane: Effect of the presence of cobalt and nickel on the deactivation behaviour of catalysts," *International Journal of Hydrogen Energy, 37(4),* pp. 3201-3212, 2012.

[19] Z. Zhang, and X.E. Verykios, "Carbon dioxide reforming of methane to synthesis gas over Ni/La2O3 catalysts," *Applied Catalysis A: General, 138(1),* pp. 109-133, 1996.

[20] Jianjun Guoa, Hui Loua, Xiaoming Zheng, "The deposition of coke from methane on a Ni/MgAl2O4 catalyst," *Carbon Volume 45, Issue 6,* p. 1314–1321, 2007.

[21] J.R. Rostrup-Nielsen, J.R. Anderson, M. Boudart (Eds.), "Catalytic steam reforming," *Catalysis: science and technology, vol. 5, Springer-Verlag, Berlin,* p. 1–117, 1984.

[22] C.H. Bartholomew and J.B. Butt, Catalysts deactivation, Amsterdam: Elsevier Science Publishers, BV, 1991.

[23] K.O. Christensen, D. Chena, R. Lødeng, A. Holmen, "Effect of supports and Ni crystal size on carbon formation and sintering during steam methane reforming," *Applied Catalysis A: General Volume 314, Issue 1,* p. 9–22, 2006.

[24] Tadeusz Borowiecki, "Nickel catalysts for steam reforming of hydrocarbons; size of crystallites and resistance to coking," *Applied Catalysis Volume 4, Issue 3,* pp. 223-231, 1982.

[25] H. S. Bengaard, J. K. Nørskov, J. Sehested, B. S. Clausen, L. P. Nielsen, A. M. Molenbroek and J. R. Rostrup-Nielsen, "Steam Reforming and Graphite Formation on Ni Catalysts," *Journal of Catalysis 209,* p. 365–384, 2002.

[26] Jianguo Zhang, Hui Wang, Ajay K. Dalai, "Effects of metal content on activity and stability of Ni-Co bimetallic catalysts for CO2 reforming of CH4," *Applied Catalysis A: General Volume 339, Issue 2,* p. 121–129, 2008.

[27] Kouta Asai, Koji Takane, Yoshiyuki Nagayasu, Shinji Iwamoto, Eriko Yagasaki and Masashi Inoue, "Decomposition of methane in the presence of carbon dioxide over Ni catalysts, Chemical Engineering Science, Volume 63, Issue 20, October 2008, Pages 5083–5088".

[28] J. Ourdar, Deactivation and Poisoning of Catalysts, Chemical Industries (Book 20), p. 270-273.

[29] H.M. Swaan, V.C.H. Kroll, G.A. Martin and C. Mirodatos, "Deactivation of supported nickel catalysts during reforming of methane by carbon dioxide," *Catalysis Today 21,* pp. 571-578, 1994.

[30] M. H. Amin, J. Tardio, S. K. Bhargava, "A Comparison Study on Carbon Dioxide Reforming of Methane Over Ni Catalysts Supported on Mesoporous SBA-15, MCM-41, KIT-6 and g-Al2O3," *Centre for Advanced Materials & Industrial Chemistry, School of Applied Sciences,* RMIT University, Melbourne, VIC 3001, Australia.

[31] J.H. Bitter, K. Seshan, and J.A. Lercher, "The State of Zirconia Supported Platinum Catalysts for CO2/CH4 Reforming," *Journal of Catalysis, 171(1),* pp. 279-286, 1997.

[32] M.A. Soria et al., "Thermodynamic and experimental study of combined dry and steam reforming of methane on Ru/ ZrO2-La2O3 catalyst at low temperature," *International Journal of Hydrogen Energy 36(23),* pp. 15212-15220, 2011.

[33] Shaobin Wang and G. Q (Max) Lu, "Carbon Dioxide Reforming of Methane To Produce Synthesis Gas over Metal-Supported Catalysts: State of the Art, Energy & Fuels 1996, 10, 896-904".

[34] S. Menada,b, P. Ferreira-Aparicioa, O. Cherifib, A. Guerrero-Ruizc and I. Rodrı´guez-Ramosa, "Designing new high oxygen mobility supports to improve the stability of RU catalysts under dry reforming of methane, Catalysis Letters Vol. 89, Nos. 1–2, July 2003".

[35] G. Xu et al., "Studies of reforming natural gas with carbon dioxide to produce synthesis gas: X. The role of CeO2 and MgO promoters," *Journal of Molecular Catalysis A: Chemical 147(1– 2),* pp. 47-54, 1999.

[36] B. M. Nagaraja, D. A.Bulushev, S. Beloshapkin and J.R. Ross, "The effect of potassium on the activity and stability of Ni–MgO–ZrO2 catalysts for the dry reforming of methane to give synthesis gas," *Catal. Today 178,* p. 132–136, 2011.

[37] G. Leendert Bezemer, J.H.B., Herman P. C. E. Kuipers, Heiko Oosterbeek, Johannes E. Holewijn, Xiaoding Xu, Freek Kapteijn, A. Jos van Dillen and Krijn P. de Jong, "Cobalt Particle Size Effects in the Fischer-Tropsch Reaction Studied with Carbon Nanofiber Supported Catalysts," *J. Am. Chem. Soc., 128 (12) ,* p. 3956–3964, 2006.

[38] M. Yu et al., "The promoting role of Ag in Ni-CeO2 catalyzed CH4-CO2 dry reforming reaction," *Applied Catalysis B: Environmental 165(0),* pp. 43-56, 2015.

[39] K. Johnsen et al., "Sorption-enhanced steam reforming of methane in a fluidized bed reactor with dolomite as -acceptor," *Chemical Engineering Science, 61(4),* pp. 1195-1202, 2006.

[40] P. Djinović et al., "Catalytic syngas production from greenhouse gasses: Performance comparison of Ru-Al2O3 and Rh-CeO2 catalysts".*Chemical Engineering and Processing: Process Intensification, 2011. 50(10): p. 1054-1062..*

[41] P.J.F. Harris, "The sintering of platinum particles in an alumina-supported catalyst".*Further transmission electron microscopy studies, Volume 97, Issue 2, February 1986, Pages 527-542.*

[42] Janina Okal and Leszek Kępiński, "Sintering of Colloidal Ru/γ-Al2O3 Catalyst in Hydrogen, Catalysis Letters March 2009, Volume 128, Issue 3, pp 331-336".

[43] Ferreira-Aparicio, P., A. Guerrero-Ruiz, and I. Rodrıgueź -Ramos, "Comparative study at low and medium reaction temperatures of syngas production by methane reforming with carbon dioxide over silica and alumina supported catalysts. Applied Catalysis A: General, 1998. 170(1): p. 177-187.".

[44] Z. Hou et al., "Production of synthesis gas via methane reforming with CO on noble metals and small amount of noble-(Rh-) promoted Ni catalysts. International Journal of Hydrogen Energy, 2006. 31(5): p. 555-561.".

[45] N. Matsui et al., "Reaction mechanisms of carbon dioxide reforming of methane with Ru-loaded lanthanum oxide catalyst. Applied Catalysis A: General, 1999. 179(1–2): p. 247-256.".

[46] M. Usman,, W.M.A. Wan Daud, and H.F. Abbas, "Dry reforming of methane: Influence of process parameters—A review. Renewable and Sustainable Energy Reviews, 2015. 45(0): p. 710-744.".

[47] K. Nagaoka, M. Okamura and K.-i. Aika, "Titania supported ruthenium as a coking-resistant catalyst for high pressure dry reforming of methane. Catalysis Communications, 2001. 2(8): p. 255-260.".

[48] Xiaohong Li, Jun Ai, Wenying Li and Dongxiong Li, "Ni-Co bimetallic catalyst for CH4 reforming with CO2, Frontiers of Chemical Engineering in China, December 2010, Volume 4, Issue 4, pp 476-480".

[49] Stavros Alexandros Theofanidis, Vladimir V. Galvita, Hilde Poelman and Guy B. Marin, "Enhanced Carbon-Resistant Dry Reforming Fe-Ni Catalyst: Role of Fe, ACS Catal., 2015, 5 (5), pp 3028–3039".

[50] Kaori Yoshida, Noorjahan Begum, Shin-ichi Ito and Keiichi Tomishige, "Oxidative steam reforming of methane over Ni/α-Al2O3 modified with trace noble metals, Applied Catalysis A: General Volume 358, Issue 2, 1 May 2009, Pages 186–192".

[51] Genira Carneiro de Araujo, Sania Maria de Lima, José Mansur Assaf, Miguel Antonio Peña, José Luís García Fierro and Maria do Carmo Rangel, "Catalytic evaluation of perovskite-type oxide LaNi1−xRuxO3 in methane dry reforming, Catalysis Today Volumes 133–135, April–June 2008, Pages 129–135".

[52] S. Damyanova, B. Pawelec, K. Arishtirova, J.L.G. Fierro, C. Sener and T. Dogu, "MCM-41 supported PdNi catalysts for dry reforming of methane, Applied Catalysis B: Environmental Volume 92, Issues 3–4, 9 November 2009, Pages 250–261".

[53] Y.G. Chen, K. Tomishige, K. Yokoyama and K. Fujimoto, "Promoting effect of Pt, Pd and Rh noble metals to the Ni0.03Mg0.97O solid solution catalysts for the reforming of CH4 with CO2, Appl. Catal. A: Gen., 165 (1997), pp. 335–347".

[54] A. Horváth, G. Stefler, O. Geszti, A. Kienneman, A. Pietraszek and L. Guczi, "Methane dry reforming with CO2 on CeZr-oxide supported Ni, NiRh and NiCo catalysts prepared by sol–gel technique: Relationship between activity and coke formation, Catalysis Today Volume 169, Issue 1, 1 July 2011, Pages 102–111".

[55] F. Basile, G. Fornasari, F. Trifiro and A. Vaccari, "Rh–Ni synergy in the catalytic partial oxidation of methane: surface phenomena and catalyst stability, Catalysis Today Volume 77, Issue 3, 15 December 2002, Pages 215–223".

[56] B. Pawelec, S. Damyanova, K. Arishtirova, J.L.G. Fierro and L. Petrov, "Structural and surface features of PtNi catalysts for reforming of methane with CO2, Applied Catalysis A: General Volume 323, 30 April 2007, Pages 188–201".

[57] Dalin Li, Yoshinao Nakagawa and Keiichi Tomishige, "Methane reforming to synthesis gas over Ni catalysts modified with noble metals, Applied Catalysis A: General Volume 408, Issues 1–2, 28 November 2011, Pages 1–24".

[58] C. Crisafulli, S. Scirè, R. Maggiore, S. Minicò and S. Galvagno, "CO2 reforming of methane over Ni–Ru and Ni–Pd bimetallic catalysts, Catalysis Letters May 1999, Volume 59, Issue 1, pp 21-26".

[59] Carmelo Crisafulli, Salvatore Scirè, Simona Minicò and Luigi Solarino, "Ni–Ru bimetallic catalysts for the CO2 reforming of methane, Applied Catalysis A: General Volume 225, Issues 1–2, 8 Feruary 2002, Pages 1–9".

[60] Yang-guang Chen, Osamu Yamazaki, Keiichi Tomishige and Kaoru Fujimoto, "Noble metal promoted Nio.03Mgo.970 solid solution catalysts for the reforming of CH4 with CO2, Catal. Lett., 39 (1996), pp. 91–95".

[61] A. Becerra, M.E. Iriarte, M. Dimitrjewits and A. Castro-Luna, "Promoting effects of rhodium on supported nickel catalysts in the dry reforming of methane, Bol. Soc. Chil. Quim., 47 (2002), pp. 385–392".

[62] M.E. Rivas, J.L.G. Fierro, M.R. Goldwasser, E. Pietri, M.J. Pérez-Zurita, A. Griboval-Constant and G. Leclercq, "Structural features and performance of LaNi1−xRhxO3 system for the dry reforming of methane, Applied Catalysis A: General Volume 344, Issues 1–2, 15 July 2008, Pages 10–19".

[63] Z.Y. Hou and T. Yashima, "Small Amounts of Rh-Promoted Ni Catalysts for Methane Reforming with CO2, Catalysis Letters September 2003, Volume 89, Issue 3, pp 193-197".

[64] S. Özkara-Aydinoğlu and A.E. Aksoylu, "CO2 reforming of methane over Pt–Ni/Al2O3 catalysts: Effects of catalyst composition, and water and oxygen addition to the feed, International Journal of Hydrogen Energy Volume 36, Issue 4, February 2011, Pages 2950–2959".

[65] M. García-Diéguez, I.S. Pieta, M.C. Herrera, M.A. Larrubia and L.J. Alemany, "Nanostructured Pt- and Ni-based catalysts for CO2-reforming of methane, Journal of Catalysis Volume 270, Issue 1, 22 March 2010, Pages 136–145".

[66] M. García-Diéguez, E. Finocchio, M.Á. Larrubia, L.J. Alemany and G. Busca, "Characterization of alumina-supported Pt, Ni and PtNi alloy catalysts for the dry reforming of methane, Journal of Catalysis Volume 274, Issue 1, 19 August 2010, Pages 11–20".

[67] G.C. Araujo, S.M. Lima, J.M. Assaf, M.A. Peña, J.L.G. Fierro, M. Carmo Rangel, G.C. Araujo, S.M. Lima, J.M. Assaf, M.A. Peña, J.L.G. Fierro and M. Carmo Rangel, "Catalysis Today Volumes 133–135, April–June 2008, Pages 129–135".

[68] M. García-Diéguez, I.S. Pieta, M.C. Herrera, M.A. Larrubia and L.J. Alemany, "Improved Pt-Ni nanocatalysts for dry reforming of methane, Applied Catalysis A: General Volume 377, Issues 1–2, 1 April 2010, Pages 191–199".

[69] M. S. Wong, "Chapter 2, Nanostructured Supported Metal Oxides: Metal Oxides Chemistry and Applications, Edited by J. L. G. Fierro, 2006, Taylor & Francis Group".

[70] Azzeddine Lekhal, Benjamin J. Glasser and Johannes G. Khinast: Chapter 16 Drying of Supported Catalysts, pp. 373-405, "Catalyst preparation Science and Engineering, Edited by J. Regalbuto, 2007, CRC Press, Taylor & Francis Group".

[71] John W. Geus, Chapter 15 Production of Supported Catalysts by Impregnation and (Viscous) Drying, pp 341-373, "Catalyst preparation Science and Engineering, Edited by J. Regalbuto, 2007, CRC Press, Taylor & Francis Group".

[72] Calvin H. Bartholomew and Robert J. Farrauto, "Fundamentals of Industrial Catalytic Processes, Second Edition, A JOHN WILEY & SONS, INC., PUBLICATION, pp. 91-101".

[73] Olaf Deutschmann, Helmut Knözinger, Karl Kochloefl and Thomas Turek, "Heterogeneous Catalysis and Solid Catalysts, 2009 Ullmann's Encyclopedia of Industrial Chemistry".

[74] Jeong Gil Seo, Min Hye Youn, Jin Suk Chung, In Kyu Song, "Effect of calcination temperature of mesoporous nickel–alumina catalysts on their catalytic performance in hydrogen production by steam reforming of liquefied natural gas (LNG), Journal of Ind. and Eng. Chemistry, Volume 16, Issue 5, 2010, pp. 795-799".

[75] Yoshio Waseda, Eiichiro Matsubara and Kozo Shinoda, "X-Ray Diffraction Crystallography, Springer-Verlag Berlin Heidelberg 2011".

[76] Stephen Bunauer, P.h. Emmett and Edward Teller, "Adsorption of Gases in Multimolecular Layers".

[77] Elliott P. Barrett, Leslie G. Joyner and Paul P. Halenda, "The Determination of Pore Volume and Area Distributions in Porous Substances. I. Computations from Nitrogen Isotherms".

[78] Paul A. Webb and Clyde Orr, "Analytical Methods in Fine Particle Technology, 1997, Micromeritics Instrument Cop., pp. 94-110, pp. 221-230".

[79] M. Fadoni and L. Lucarelli, "Temperature programmed desorption, reduction, oxidation and flow chemisorption for the characterisation of heterogeneous catalysts. Theoretical aspects, instrumentation and applications, Studies in surface science and catalysis 120A:177-225 Desember 1999".

[80] G.Delahay, "Ph.D. Thesis, Université de Toulouse, France 1991".

[81] M. Khoshtinat Nikoo and N.A.S. Amin, "Thermodynamic analysis of carbon dioxide reforming of methane in view of solid carbon formation Fuel Processing Technology Volume 92, Issue 3, March 2011, Pages 678–691".

[82] Y. Vafaeian, M. Haghighi and S. Aghamohammadi, "Ultrasound assisted dispersion of different amount of Ni over ZSM-5 used as nanostructure catalyst for hydrogen production via CO2 reforming methane, Energy Conversion and management, 76 (2013) 1093-1103.".

[83] Pil Kim, Younghun Kim, Heesoo Kim, In Kyu Song and Jongheop Yi, "Synthesis and characterization of mesoporous alumina with nickel, Applied Catalysis A: General 272 (2004) pp. 157–166".

[84] Chiuping Li and Yu-Wen Chen, "Temperature-programmed-reduction studies of nickel, Thermochimica Acta 256 (1995) pp. 457-465".

[85] G. Poncelet, M.A. Centeno and R. Molina, "Characterization of reduced α-alumina-supported nickel catalysts by spectroscopic and chemisorption measurements, Applied Catalysis A: General, Volume 288, Issues 1–2, 15 July 2005, Pages 232–242".

[86] Andrea Álvarez M, Miguel Ángel Centeno and José Antonio Odriozola, "Ru–Ni Catalyst in the Combined Dry-Steam Reforming of Methane: The Importance in the Metal Order Addition, Topics in Catalysis, February 2016, Volume 59, Issue 2, pp 303–313".

[87] Chao Chen, Wha-Seung Ahn, "CO2 capture using mesoporous alumina prepared by a sol–gel process, Chemical Engineering Journal Volume 166, Issue 2, 15 January 2011, Pages 646–651".

[88] P. A. Sermon and G. C. Bond, "Hydrogen Spillover, Catalysis Reviews: Science and Engineering, Volume 8, Issue 1, 1974, pp. 211-239".

[89] R. Molina and G. Poncelet, "r-Alumina-Supported Nickel Catalysts Prepared with Nickel Acetylacetonate. 2. A Study of the Thermolysis of the Metal Precursor, J. Phys. Chem. B 1999, 103, 11290-11296".

[90] Neda Mazinanian, Yolanda Hedberg, Inger Odnevall Wallinder, "Nickel release and surface characteristics of fine powders of nickel metal and nickel oxide in media of relevance for inhalation and dermal contact, Regulatory Toxicology and Pharmacology, Volume 65, Issue 1, February 2013, Pages 135–146".

[91] Guohui Li, Linjie Hu, Josephine M. Hill, "Comparison of reducibility and stability of alumina-supported, Applied Catalysis A: General 301 (2006) 16–24".

[92] Jarrod Newnham, Kshudiram Mantri, Mohamad Hassan Amin, James Tardio and Suresh K. Bhargava, "Highly stable and active Ni-mesoporous alumina catalysts for dry reforming of methane, Volume 37, Issue 2, January 2012, International Journal of Hydrogen Energy Pages 1454–1464".

[93] Wang, H. Y. and E. Ruckenstein, "Partial Oxidation of Methane to Synthesis Gas over MgO- and SiO2-Supported Rhodium Catalysts. (1999) J. Catal. 186(1): 181-187.".

[94] Haynes, D. J., D. A. Berry, et al., " Catalytic partial oxidation of n-tetradecane using Rh and Sr substituted pyrochlores: Effects of sulfur, (2009), Catal. Today 145(1-2): 121-126".

[95] W. Curstis Conner, Jr., and John L. Falconer, "Spillover in Heterogeneous Catalysis, Chem. Rev. Febuary 1995, 85, pp. 759-788".

[96] Nader Rahemi, Mohammad Haghighi, Ali Akbar Babaluo, Mahdi Fallah Jafari and Pooya Estifaee, "Synthesis and physicochemical characterization of Ni/Al2O3 ZrO2 nano catalyst prepared via impregnation method and treated with non-thermal plasma for CO2 reforming of CH4, Journal of Ind. and Eng. Chem. Volume 19, 2013, pp. 1566-1576".

[97] Shaobin Wang and G.Q Lu, "Reforming of methane with carbon dioxide over Ni/Al2O3 catalysts: Effect of nickel precursor, Applied Catalysis A: General Volume 169, Issue 2, 11 May 1998, Pages 271–280".

[98] A.S.A. Al-Fatesh and A.H. Fakeeha, "Effects of calcination and activation temperature on dry reforming catalysts, Journal of Saudi Chemical Society, Volume 16, Issue 1, January 2012, Pages 55–61".

[99] E.L. Jablonski, I. Schmidhalter, S.R. de Miguel, O.A. Scelza, A.A. Castro, "Dryreforming of methane on Pt/Al2O3–alkaline metal catalysts, 2nd MercosurCongress on Chemical Engineering, Rio de Janeiro, 2005, pp. 1–13".

[100] Minhua Zhang, Dang-guo Cheng, Yue-ping Zhang, "Carbon Dioxide Reforming of Methane over a Novel Ni/Al2O3 Catalysts," *Prepr. Pap.-Am. Chem. Soc., Div. Fuel Chem. 49 (1), 189,* 2004.

[101] Wenjuan Shan, Mengfei Luo, Pinliang Ying, Wenjie Shen, Can Li, "Reduction property and catalytic activity of Ce1−XNiXO2 mixed oxide catalysts for CH4 oxidation, Applied Catalysis A: General, Volume 246, Issue 1, 25 June 2003, Pages 1–9".

[102] Z. Hou and T. Yashima, "Meso-porous Ni/Mg/Al catalysts for methane reforming with CO2. Applied Catalysis A: General Volume 261, Issue 2, 30 April 2004, Pages 205–209".

[103] G.R. Gavalas, C. Phichitkul and G.E. Voecks, "Structure and activity of NiOα-Al2O3 and NiOZrO2 calcined at high temperatures: I. Structure, Journal of Catalysis, Volume 88, Issue 1, July 1984, Pages 54-64".

[104] Andries Q.M. Boon 1, H.Michiel Huisman, John W. Geus, "Influence of surface oxygen vacancies on the catalytic activity of copper oxide Part 2. Oxidation of methane, Journal of Molecular Catalysis Volume 75, Issue 3, 1 October 1992, Pages 293-303".

[105] Andries Q.M. Boon 1, H.Michiel Huisman, John W. Geus, "Influence of surface oxygen vacancies on the catalytic activity of copper oxide Part 2. Oxidation of methane, Volume 75, Issue 3, 1 October 1992, Pages 293-303".

Appendix A: Calculation for catalyst synthesis

Metal	Precursor	Chemical formula	Molecular weight (g/mol)	Metal basis (%)	Dilution factor (Df)
Ni	Nickel(II) nitrate hexahydrate	$N_2NiO_6 * 6H_2O$	290.79	99.999	1
Pt	Tetraamminplatinum(II) nitrate	$H_{12}N_6O_6Pt$	387.21	≥50	0.5
Pd	Palladium(II) nitrate hydrate	$N_2O_6Pd * xH_2O$	230.43	-	1
Rh	Rhodium(III) nitrate hydrate	$N_3O_9Rh * xH_2O$	288.92	36	0.36
Ru	Ruthenium(III) nitrosyl nitrate	$HN_4O_{10}Ru$	318.10	1-2	0.015

Water in the precursors of Pd and Rh was not taken into consideration when calculating the amount of mixture volume for incipient wetness.

Formulas for calculation:

$$Ni(weight\ fraction) = \frac{Ni(g)}{Support(g)+Ni(g)+NM(g)} = a \quad \textbf{(A.1)}$$

$$NM(weight\ fraction) = \frac{NM(g)}{Support(g)+Ni(g)+NM(g)} = b \quad \textbf{(A.2)}$$

Combining A.1 and A.2 to find noble metal (NM) and Ni weight fractions in grams:

$$NM(g) = \frac{b*support(g)}{(1-a)(1-b)-\frac{ab}{1-a}} \quad \textbf{(A.3)}$$

$$Ni(g) = \frac{a*Support(g)+a*NM(g)}{1-a} \quad \textbf{(A.4)}$$

$$Metal\ Precursor(g) = \frac{M_{w,precursor}(\frac{g}{mol})}{M_{w,metal}(\frac{g}{mol})*Df} * Metal(g) \quad \textbf{(A.5)}$$

$$Amount\ of\ Water\ in\ Precursor(ml) = \frac{N_2NiO_6*6H_2O(g)}{M_{w,Niprecursor}(\frac{g}{mol})*\rho_{H_2O}(\frac{g}{ml})} * 6 * M_{w,H_2O}(\frac{g}{mol}) \quad \textbf{(A.6)}$$

Incipient wetness mixture volume to be mixed with the support:

Volume of water(ml) + volume precursor(ml) = Average pore volume of support(ml) – Amount of Water in Precursor (ml)

Example 0.5Pt12Ni/SCCa:

Theoretical amount support and metal loading fractions: Support(g) = 10g, a = 0.005, b = 0.12

Pt(g) = $\frac{0.005*10}{(1-0.12)*(1-0.005)-\frac{0.12*0.005}{1-0.12}} = 0.0571$g

Ni(g) = $\frac{0.12*10+0.12*0.0571}{1-0.12} = 1.3714$g

Pt precursor(g) = $\frac{387.21}{195.084*0.5} * 0.0571 = 0.2267$g

Ni precursor(g) = $\frac{290.79}{58.693} * 1.3714 = 6.7945$g

Incipient volume = $1{,}0491\ \mathrm{ml/g} * 10\mathrm{g} = 10.49\mathrm{ml}$

Amount of Water in Ni precursor(ml) = $\frac{6.7945}{1*290.79} * 6 * 18.0153 = 2.52\mathrm{ml}$

Mixture Volume = Volume of water + metal precursors = 10.49 – 2.52 = 7.97ml

To prepare the 0.5Pt12Ni/SCCa catalyst 10g of support was used. 0.2256g of Pt precursor and 6.7945g of Ni precursor was added to the glassware before adding deionized water up to marked volume of 7.97ml.